



Deposited via The University of York.

White Rose Research Online URL for this paper:

<https://eprints.whiterose.ac.uk/id/eprint/140146/>

Version: Accepted Version

---

**Article:**

Oswald, Matthew Charles William, Brooks, Paul S., Zwart, Maarten F. et al. (2018)  
Reactive Oxygen Species Regulate Activity-Dependent Neuronal Plasticity in Drosophila.  
eLife. e39393. ISSN: 2050-084X

<https://doi.org/10.7554/eLife.39393>

---

**Reuse**

This article is distributed under the terms of the Creative Commons Attribution (CC BY) licence. This licence allows you to distribute, remix, tweak, and build upon the work, even commercially, as long as you credit the authors for the original work. More information and the full terms of the licence here:

<https://creativecommons.org/licenses/>

**Takedown**

If you consider content in White Rose Research Online to be in breach of UK law, please notify us by emailing [eprints@whiterose.ac.uk](mailto:eprints@whiterose.ac.uk) including the URL of the record and the reason for the withdrawal request.

1 **Title:** Reactive Oxygen Species Regulate Activity-Dependent Neuronal Plasticity in *Drosophila*

2  
3 **Authors:** Matthew C. W. Oswald<sup>1\*</sup>, Paul S. Brooks<sup>1</sup>, Maarten F. Zwart<sup>2</sup>, Amrita Mukherjee<sup>1</sup>, Ryan J. H.  
4 West<sup>3,4</sup>, Carlo Giachello<sup>3</sup>, Khomgrit Morarach<sup>1</sup>, Richard A. Baines<sup>3</sup>, Sean T. Sweeney<sup>4</sup>, Matthias  
5 Landgraf<sup>1\*</sup>

6 \*Correspondence to: [mo364@cam.ac.uk](mailto:mo364@cam.ac.uk) and [ml10006@cam.ac.uk](mailto:ml10006@cam.ac.uk)

7  
8  
9 **Affiliations:**

10 <sup>1</sup> University of Cambridge, Department of Zoology, Downing Street, Cambridge, CB2 3EJ, United  
11 Kingdom

12 <sup>2</sup> HHMI Janelia Research Campus, Ashburn, VA, 20147, USA

13 <sup>3</sup> Faculty of Biology, Medicine and Health, University of Manchester, Oxford Road, Manchester, M13  
14 9PT, UK

15 <sup>4</sup> Department of Biology, University of York, Heslington York YO10 5DD, United Kingdom

16  
17  
18  
19  
20  
21 **Abstract:**

22 Reactive oxygen species (ROS) have been extensively studied as damaging agents associated with  
23 ageing and neurodegenerative conditions. Their role in the nervous system under non-pathological  
24 conditions has remained poorly understood. Working with the *Drosophila* larval locomotor network,  
25 we show that in neurons ROS act as obligate signals required for neuronal activity-dependent  
26 structural plasticity, of both pre- and postsynaptic terminals. ROS signaling is also necessary for  
27 maintaining evoked synaptic transmission at the neuromuscular junction, and for activity-regulated  
28 homeostatic adjustment of motor network output, as measured by larval crawling behavior. We  
29 identified the highly conserved Parkinson's disease-linked protein DJ-1 $\beta$  as a redox sensor in neurons  
30 where it regulates structural plasticity, in part via modulation of the PTEN-PI3Kinase pathway. This  
31 study provides a new conceptual framework of neuronal ROS as second messengers required for  
32 neuronal plasticity and for network tuning, whose dysregulation in the ageing brain and under  
33 neurodegenerative conditions may contribute to synaptic dysfunction.

34

35  
36  
37  
38  
39  
40  
41  
42  
43  
44  
45  
46  
47  
48  
49  
50  
51  
52  
53  
54  
55  
56  
57  
58  
59  
60  
61  
62  
63  
64  
65  
66  
67  
68  
69  
70  
71  
72  
73  
74  
75  
76  
77

## Introduction

Levels of reactive oxygen species (ROS) in the brain increase with ageing and high levels of ROS are a hallmark of neurodegeneration, including Alzheimer's and Parkinson's disease (Höhn and Grune, 2013; Martins et al., 1986; Spina and Cohen, 1989) for review see (Milton and Sweeney, 2012). Mitochondria are a significant source of ROS, which form as obligate byproducts of respiratory ATP synthesis by 'leakage' of the electron transport chain, thus leading to the generation of superoxide anions ( $O_2^-$ ) and hydrogen peroxide ( $H_2O_2$ ) (Halliwell, 1992). Implicit in their name, ROS are highly reactive, containing one or more unpaired electrons, with the potential to modify and damage by oxidation proteins, lipids and DNA (Gladyshev, 2014; Harman, 1956; Stuart et al., 2014). Importantly, ROS have also been recognized as signaling molecules in metabolic pathways (Liemburg-Apers et al., 2015) and controlling the activity of transcription factors such as AP-1 and Nrf2 (Jindra et al., 2004; Soriano et al., 2009). Moreover, several kinase signaling pathways are enhanced by ROS, either by oxidation of kinase interacting modulators, such as thioredoxin or glutathione-S-transferases (Adler et al., 1999; Saitoh et al., 1998), or through inhibition of counteracting phosphatases, e.g. PTEN, by oxidation of the active site cysteine residue (Finkel, 2011; Stuart et al., 2014; Tonks, 2005).

We previously showed in a model for lysosomal storage diseases that ROS can regulate neuromuscular junction (NMJ) structure (Milton et al., 2011). NMDA receptor stimulation can lead to ROS generation (Bindokas et al., 1996; Brennan et al., 2009; Dugan et al., 1995), and in hippocampal and spinal cord slices ROS have been shown sufficient and necessary for inducing 'Hebbian' forms of plasticity (LTP) (Kamsler and Segal, 2003a; Kamsler and Segal, 2003b; Klann, 1998; Knapp and Klann, 2002; Lee et al., 2010). Conversely, disturbing the ROS balance by over-expression of the scavenger superoxide dismutase caused defects in hippocampal LTP and learning paradigms in mice (Gahtan et al., 1998; Levin et al., 1998; Thiels et al., 2000). Recent studies have linked increased ROS levels with neurodevelopmental conditions such as schizophrenia, bipolar and autism spectrum disorders (Do et al., 2015; Steullet et al., 2017).

Here, we set out to investigate potential roles for ROS in the nervous system under non-pathological conditions, which are much less well understood. The brain is arguably the most energy demanding organ and mitochondrial oxidative phosphorylation is a major source of ROS (Attwell and Laughlin, 2001; Hallermann et al., 2012; Zhu et al., 2012). We therefore asked whether neurons might utilize mitochondrial metabolic ROS as feedback signals to mediate activity-regulated changes. As an experimental model we used the motor system of the fruitfly larva, *Drosophila melanogaster*, which allows access to uniquely identifiable motoneurons in the ventral nerve cord and their specific body wall target muscles (Kohsaka et al., 2012). We established an experimental paradigm for studying activity-regulated structural adjustments across an identified motoneuron, quantifying changes at both pre- and postsynaptic terminals. We show that thermogenetic neuronal over-activation leads to the generation of ROS at presynaptic terminals, and that ROS signaling is necessary and sufficient for the activity-regulated structural adjustments. As a cellular ROS sensor we identified the conserved redox sensitive protein DJ-1 $\beta$ , a homologue of vertebrate DJ-1 (PARK7) (Meulener et al., 2005), and the phosphatase and tensin homolog (PTEN) and PI3kinase as downstream effectors of activity-ROS-mediated structural plasticity. We find that ROS signaling is

78 also required for maintaining constancy of evoked transmission at the neuromuscular junction (NMJ)  
79 with a separate ROS pathway regulating the amplitude of spontaneous vesicle release events.  
80 Behaviourally, ROS signaling is required for the motor network to adjust homeostatically to return to  
81 a set crawling speed following prolonged overactivation.

82 In summary, this study establishes a new framework for studying ROS in the nervous system:  
83 as obligatory regulators that inform neurons about their activation status, and as obligatory  
84 mediators of activity-induced plasticity, both structural and physiological.

85  
86  
87

## 88 **Results**

89

### 90 **Structural plasticity of synaptic terminals is regulated by neuronal activity**

91 Our aim was to explore roles for activity-regulated ROS signaling in the nervous system under non-  
92 pathological conditions. Working with the *Drosophila* larval neuromuscular system allowed us to  
93 target manipulations to identified nerve cells *in vivo* that manifest structural and functional plasticity  
94 (Frank et al., 2013; Tripodi et al., 2008; Wolfram and Baines, 2013; Zwart et al., 2013). We focused  
95 on two well characterized motoneurons, 'aCC' and 'RP2', which jointly innervate the dorsal acute  
96 muscle 1 (DA1) (Figure 1A) (Baines et al., 1999; Baines et al., 2001; Bate, 1993; Choi et al., 2004;  
97 Hoang and Chiba, 2001; Landgraf et al., 2003; Sink and Whittington, 1991). First, we characterized  
98 activity-regulated morphological changes at the presynaptic neuromuscular junction (NMJ) and, in  
99 the central nervous system (CNS), the branched postsynaptic dendritic arbors that receive input  
100 from premotor interneurons (Baines et al., 1999; Schneider-Mizell et al., 2016; Zwart et al., 2013). A  
101 simple method for increasing activity in the larval locomotor network is to increase ambient  
102 temperature from the default standard of 25°C to 29°C or 32°C. Sigrist et al. (2003) and Zhong and  
103 Wu (2004) previously demonstrated this to trigger increased locomotor activity and to result in  
104 increased varicosity (bouton) number at presynaptic NMJs (Sigrist et al., 2003; Zhong and Wu, 2004).  
105 We were able to reproduce and extend these findings: rearing larvae at higher ambient  
106 temperatures results in NMJs having more boutons than controls by the third instar wandering  
107 stage, 100 hrs after larval hatching (ALH) (grey data in Figure 1B-C, compare 25°C with 29°C and 32°C  
108 conditions). To complement these systemic manipulations and to exclude potential non-specific  
109 effects we turned to a cell-specific activation paradigm of selectively overactivating the aCC and RP2  
110 motoneurons via targeted mis-expression of the warmth-gated cation channel dTrpA1. Expression of  
111 dTrpA1 in neurons is a well established method for temperature controlled neuronal overactivation  
112 (Hamada et al., 2008; Oswald et al., 2015). For larval motoneurons in particular, Pulver and  
113 colleagues demonstrated that dTrpA1 is activated above 24°C, at 25°C leading to action potential  
114 firing frequencies of 9-12 Hz (moderate activation) and 22-30 Hz at 27°C (stronger activation) (Pulver  
115 et al., 2009). These activation levels are within the physiological range of larval motoneurons,  
116 thought to operate at approximately 42 Hz during muscle contraction cycles (Chouhan et al., 2010).  
117 Similar to the systemic manipulations, we found that cell-specific thermogenetic dTrpA1 activation  
118 of single motoneurons also led to titratable increases in bouton number at presynaptic NMJs (blue  
119 data in Figure 1B-C). Note that these cell-specific dTrpA1-mediated activity manipulations were

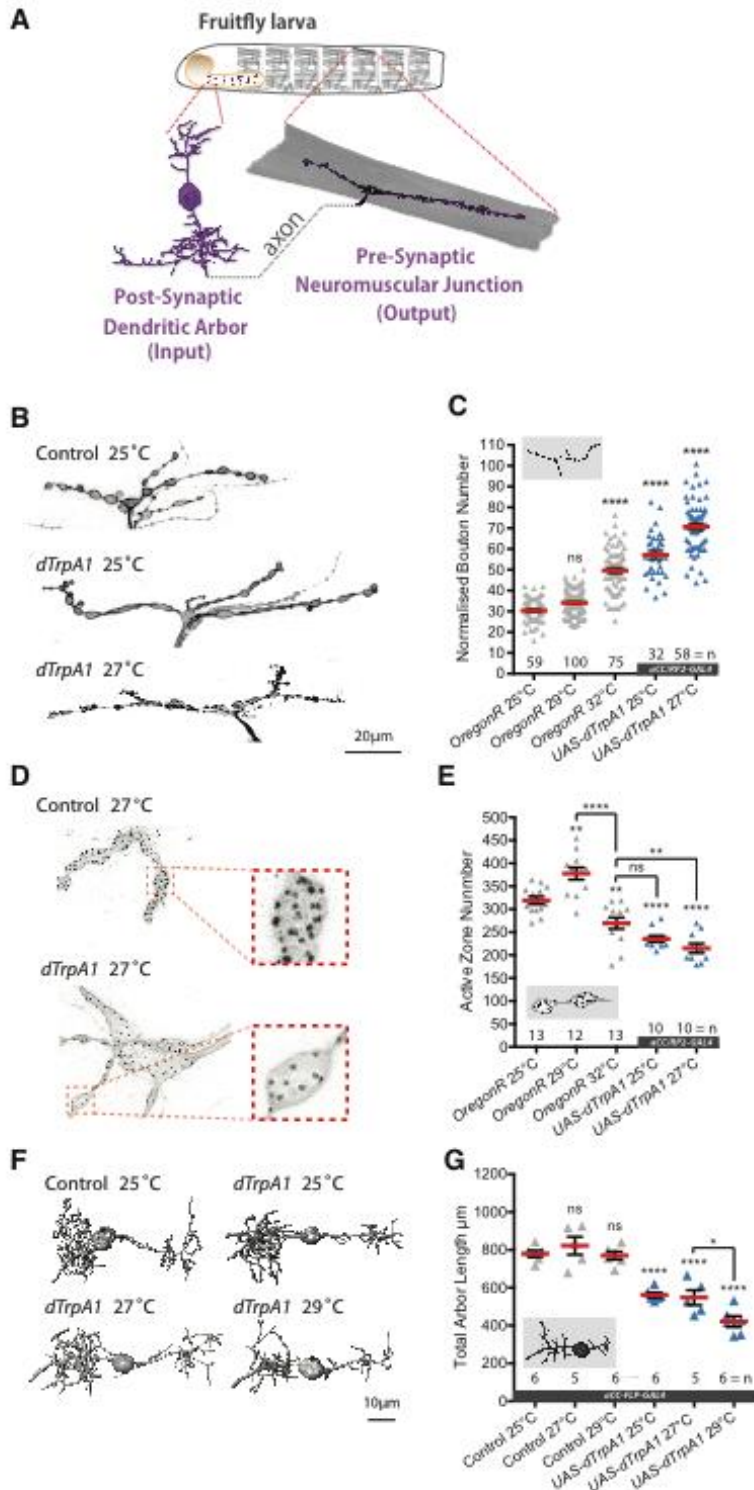
120 carried out at 25°C and 27°C, sufficient to activate dTrpA1 expressing neurons, but otherwise not  
121 causing significant changes in NMJ morphology in non-expressing motoneurons (Tsai et al., 2012).

122 Next, we quantified synapse number at the presynaptic NMJ on muscle DA1, measured by  
123 active zones (visualized with the nc82 antibody against the active zone protein Bruchpilot (Wagh et  
124 al., 2006)). This describes a more complex relationship. As previously published, a moderate increase  
125 in activity, e.g., rearing larvae at 29°C, causes both more boutons and also more active zones to be  
126 formed, potentiating transmission at the NMJ (Sigrist et al., 2003). In contrast, further increases in  
127 network activity, as effected by rearing larvae at 32°C or by cell-specific dTrpA1-mediated  
128 motoneuron activation at increasing temperatures led to progressive active zone reductions (Figure  
129 1D, E).

130 We then looked at activity-regulated structural changes of the postsynaptic dendritic arbor  
131 of the aCC motoneuron, which is known to be plastic during embryonic and larval stages (Hartwig et  
132 al., 2008; Tripodi et al., 2008). To this end, we targeted GAL4 and dTrpA1 expression to individual  
133 aCC motoneurons (Ou et al., 2008). Morphometric analysis revealed that the size of the aCC  
134 postsynaptic dendritic arbor decreased with rising levels of temperature-gated dTrpA1 activity  
135 (Figure 1F, G). We and others previously showed that dendritic length of these neurons correlates  
136 with input synapse number and synaptic drive (Schneider-Mizell et al., 2016; Zwart et al., 2013).

137 In summary, we find that the synaptic terminals of larval motoneurons undergo titratable  
138 structural changes in response to neuronal overactivation. Postsynaptic dendritic arbor size, and by  
139 inference synapse number and synaptic drive (Zwart et al., 2013), negatively correlate with  
140 activation levels. At the presynaptic NMJ, synapse number also correlates negatively with activation  
141 level - bar a narrow low level activity window that can lead to potentiation (Ataman et al., 2008;  
142 Piccioli and Littleton, 2014; Sigrist et al., 2003). Boutons provide an additional anatomical readout  
143 for NMJ plasticity, increasing in number with levels of activity. However, no functional significance of  
144 bouton number and size has been documented and changes in these bouton parameters are not  
145 predictive of changes in synaptic transmission (Campbell and Ganetzky, 2012).

146



147  
 148  
 149  
 150  
 151  
 152  
 153  
 154

**Figure 1: Adaptive structural synaptic plasticity at motoneuron input and output terminals in response to increased neuronal activity.** (A) Graphical illustration of a stereotypical larval motoneuron (MN) (adapted from Kohsaka et al. (2012)). Pre-motor interneurons make synaptic connections with the MN dendritic arbor (input) in the larval ventral nerve cord (equivalent of mammalian spinal cord). The MN extends an axonal projection into the periphery where it connects with a target muscle via an NMJ, characterized by varicose swellings (boutons) each containing multiple individual neurotransmitter release sites (active zones). (B and C) Representative images of

155 muscle DA1 [muscle 1 according to (Crossley, 1978)] NMJs from 3<sup>rd</sup> instar larvae (100hrs ALH). Dot-  
156 plot quantification shows NMJ bouton number increases in response to systemic and cell-specific  
157 activity increases. (D and E) Active zone number increases following low-level overactivation (29°C),  
158 but progressively reduces upon stronger overactivation. (F and G) Digital reconstructions and dot  
159 plots show that overactivation leads to reduced total dendritic arbor length of aCC motoneurons  
160 (24hrs ALH). 'aCC/RP2-GAL4' expresses GAL4 in all, 'aCC-FLP-GAL4' in single aCC and RP2  
161 motoneurons (see Online Methods for details); 'Control' in (B-G) is heterozygous aCC/RP2-GAL4 or  
162 aCC-FLP-GAL4, achieved by crossing the respective GAL4 line to Oregon-R wild type. Mean +/- SEM,  
163 ANOVA, ns = not significant, \*P<0.05, \*\*P<0.01, \*\*\*P<0.001, \*\*\*\*P<0.0001, n = replicate number.  
164 Comparisons with control are directly above data points.

165  
166

### 167 **Neuronal overactivation leads to ROS generation in presynaptic terminals.**

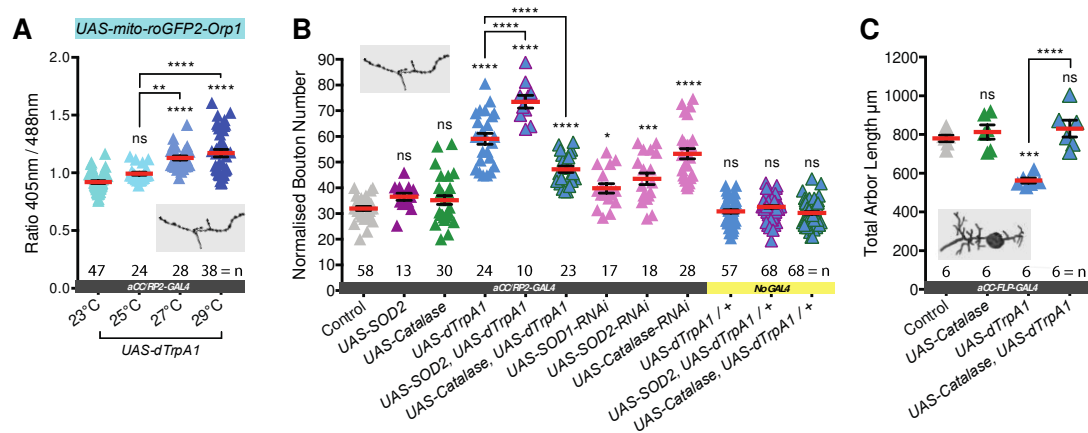
168 Next, we asked if *in vivo* overactivation of individual motoneurons is associated with increased ROS  
169 levels, as reported for hippocampal neurons in culture (Hongpaisan et al., 2004). To this end, we co-  
170 expressed in aCC and RP2 motoneurons the mitochondrion-targeted ratiometric ROS reporter *UAS-*  
171 *mito-roGFP2-Orp1* (Gutscher et al., 2009) along with *UAS-dTrpA1*. We focused on mitochondria at  
172 the muscle DA1 NMJs of wandering third instar larvae (100 hrs ALH). Quantification shows a clear  
173 trend of increasing temperature and dTrpA1-mediated activation resulting in progressively greater  
174 mean oxidation levels of this ROS sensor in mitochondria at the NMJ (Figure 2A). These data show  
175 that *in vivo* dTrpA1-mediated overactivation of *Drosophila* larval motoneurons leads to increased  
176 mitochondrial ROS at presynaptic NMJs.

177  
178

### 179 **Activity generated ROS regulate structural plasticity at synaptic terminals**

180 We then tested whether or not ROS are required for activity-dependent structural synaptic terminal  
181 plasticity. To this end we increased neuronal activity in the aCC and RP2 motoneurons via dTrpA1  
182 expression, rearing larvae at 25°C, the lower threshold of dTrpA1 activation that leads to activity-  
183 dependent changes of synaptic terminals. At the same time we additionally over-expressed in these  
184 neurons ROS scavenging enzymes: Superoxide Dismutase 2 (SOD2), which catalyses O<sub>2</sub><sup>-</sup> to H<sub>2</sub>O<sub>2</sub>  
185 reduction; or Catalase, which converts H<sub>2</sub>O<sub>2</sub> into H<sub>2</sub>O and O<sub>2</sub>. Over-expression of either ROS  
186 scavenger enzyme alone showed no effect on NMJ bouton number (Figure 2B). For Catalase over-  
187 expression we further quantified active zone number at the NMJ and dendritic arbor size and there  
188 too found this indistinguishable from controls (Figure 2C, 3B). In contrast, co-expression of *UAS-*  
189 *Catalase* with *UAS-dTrpA1* significantly counteracted changes in bouton and active zone number  
190 otherwise caused by dTrpA1-mediated neuronal overactivation (25°C) (Figure 2B, 3B). Similarly, at  
191 the motoneuron input terminals in the CNS, Catalase co-expression rescued dendritic arbor size  
192 (Figure 2C). Conversely, SOD2 co-expression enhanced the dTrpA1-mediated increase of bouton  
193 number at the NMJ, presumably by potentiating conversion of activity-generated increase of O<sub>2</sub><sup>-</sup> into  
194 H<sub>2</sub>O<sub>2</sub> (Figure 2B). We next asked if increasing neuronal ROS was sufficient to invoke structural  
195 plasticity in the absence of dTrpA1 activity manipulations. Indeed, cell-specific RNAi knock down of  
196 any one of three endogenous ROS scavengers, SOD1, SOD2 or Catalase, led to NMJs with increased  
197 bouton number, in agreement with a prior study by Milton et al. (2011), who had demonstrated

198 oxidative stress causing NMJ growth. These structural NMJ changes are similar to those produced by  
 199 neuronal overactivation (Figure 2B) and implicate ROS, specifically  $H_2O_2$ , as a signal for regulating  
 200 activity-dependent structural plasticity at input and output terminals.



201  
 202

203 **Figure 2: Neuronal activation leads to generation of synaptic ROS that regulate structural**  
 204 **plasticity at input and output terminals.** (A) Elevated cell-specific activity increases mitochondrial  
 205 ROS production at NMJs. Dot plots of mitochondrion-targeted ratiometric  $H_2O_2$  sensor (UAS-mito-  
 206 roGFP2-Orp1 (Gutschner et al., 2009)) in wandering 3<sup>rd</sup> instar larval NMJs (100hrs ALH) at 23°C  
 207 (control, dTrpA1 inactive), 25°C (moderate), 27°C (strong) and 29°C (very strong) dTrpA1-mediated  
 208 overactivation. (B) Bouton number at the NMJ is increased by UAS-dTrpA1-mediated overactivation.  
 209 This is exacerbated by co-expression of UAS-SOD2 (converts  $O_2^-$  to  $H_2O_2$ ) and rescued by expression of  
 210 the  $H_2O_2$  scavenger UAS-Catalase. Cell-specific ROS elevation by scavenger knockdown is sufficient to  
 211 induce NMJ elaboration. aCC/RP2-GAL4, 'Control' is aCC/RP2-GAL4 alone. (C) Total dendritic arbor  
 212 length is reduced by single cell overactivation, but rescued by co-expression of the  $H_2O_2$  scavenger  
 213 UAS-Catalase (aCC motoneurons, 24hr ALH). aCC-FLP-GAL4, 'Control' is aCC-FLP-GAL4 alone,  
 214 heterozygous, achieved by crossing the GAL4 driver to Oregon-R wild type flies. Larvae were reared  
 215 at 25°C unless indicated otherwise. Mean +/- SEM, ANOVA, ns = not significant, \*P<0.05, \*\*P<0.01,  
 216 \*\*\*P<0.001, \*\*\*\*P<0.0001, n = replicate number.

217

218

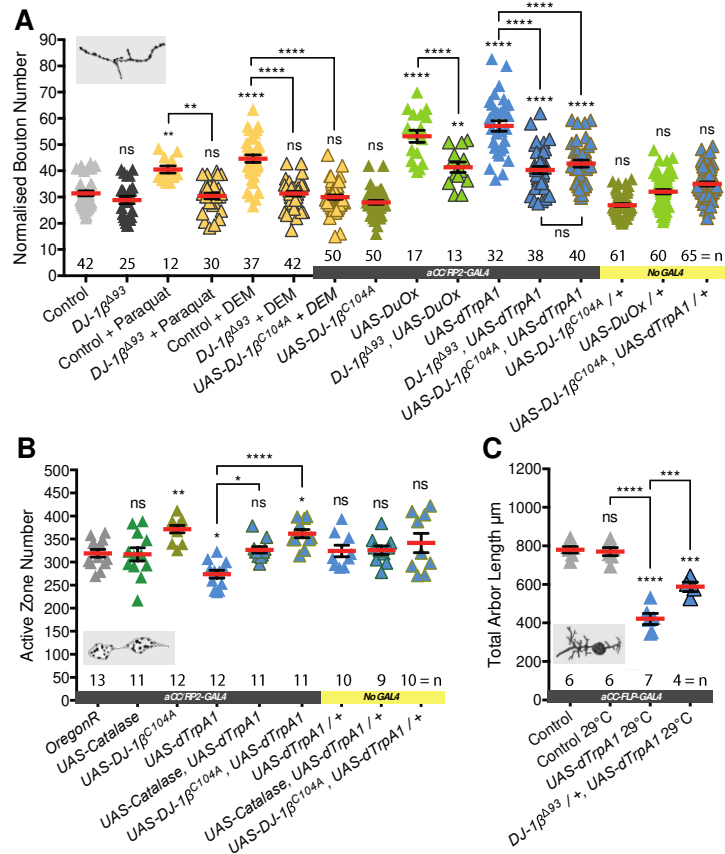
### 219 DJ-1 $\beta$ acts as a ROS sensor in neurons

220 We then investigated how neurons might sense changes in activity-induced ROS levels. ROS are  
 221 known to post-translationally modify many different proteins, principally on cysteine or methionine  
 222 residues, including transcription factors, cytoskeletal proteins, cell adhesion molecules and  
 223 phosphatases (for review see (Milton and Sweeney, 2012)). We identified DJ-1 $\beta$ , the fly ortholog of  
 224 DJ-1 (PARK7), as a candidate ROS sensor. DJ-1 codes for a highly conserved, ubiquitously expressed  
 225 redox-sensitive protein, that protects against oxidative stress and regulates mitochondrial function  
 226 (Ariga et al., 2013; Nagakubo et al., 1997). A mutant allele is also linked to a rare form of familial  
 227 Parkinsonism (Bonifati et al., 2003). DJ-1 null mutants are viable without any conspicuous defects  
 228 and adult flies have been reported to have increased sensitivity to oxidative stress, e.g., as induced  
 229 by exposure to paraquat or  $H_2O_2$  (Meulener et al., 2005). We found that DJ-1 $\beta$  null mutant (DJ-1 $\beta^{\Delta 93}$ )  
 230 larvae develop normally, indistinguishable from wild type controls, and have structurally normal

231 NMJs (Figure 3A and Figure 3-supplement 1). Interestingly, in larvae homozygous for the *DJ-1*<sup>Δ93</sup>  
232 null mutation, NMJs fail to respond to elevated ROS levels and do not generate additional boutons,  
233 as typical for controls when feeding 10mM paraquat, which causes elevated O<sub>2</sub><sup>-</sup> release from  
234 mitochondrial complex 1, or 10mM Diethyl maleate (DEM), which inactivates the ROS scavenger  
235 glutathione (Milton et al., 2011) (Figure 3A). Similarly, loss of DJ-1β also significantly rescues NMJ  
236 bouton addition phenotypes induced by targeted expression of the ROS generator Duox in aCC and  
237 RP2 motoneurons, or their dTrpA1-mediated overactivation (Figure 3A). *DJ-1*<sup>Δ93</sup> mutant larvae also  
238 failed to produce the presynaptic bouton and active zone addition that result from raising larvae at  
239 29°C (Sigrist et al., 2003) (Figure 3 – supplement 2). The neuronal requirement for *DJ-1*β was further  
240 tested via rescue experiments where neuronal *UAS-DJ-1*β miss-expression in a *DJ-1*β null-mutant  
241 background proved sufficient to re-establish sensitivity to DEM (see Figure 3 – supplement 3). Next,  
242 we cell-autonomously changed the ability of DJ-1β to act as a redox sensor. DJ-1 is known to form  
243 dimers (Lin et al., 2012a). We expressed in aCC and RP2 motoneurons a dominant-acting mutant  
244 form of DJ-1β that is non-oxidizable at the conserved cysteine 104, *UAS-DJ-1*β<sup>C104A</sup> (Meulener et al.,  
245 2006). Expression of DJ-1β<sup>C104A</sup> abrogated ROS-induced (following DEM feeding) as well as dTrpA1  
246 activity-mediated NMJ structural adjustment, both with respect to bouton number (Figure 3A) and  
247 active zone number (Figure 3B). Looking at activity-dependent structural plasticity of the  
248 postsynaptic dendritic arbor, we found this is sensitive to *DJ-1*β levels; halving the copy number of  
249 *DJ-1*β (in *DJ-1*β<sup>Δ93</sup>/+ heterozygotes) was sufficient to significantly suppress dTrpA1-mediated changes  
250 to dendritic arbor size (Figure 3C).

251 In summary, these data show that DJ-1β is necessary for activity-induced structural changes,  
252 compatible with DJ-1β functioning as a sensor for ROS. DJ-1β appears to be required in motoneurons  
253 for increasing NMJ bouton and active zone numbers in response to mild overactivation regimes that  
254 lead to potentiation of transmission at the NMJ (raising larvae at 29°C) (Sigrist et al., 2003). At higher  
255 levels, as induced by dTrpA1-mediated overactivation, DJ-1β is also necessary in motoneurons,  
256 though under these conditions for decreasing active zone numbers at the NMJ and the size of  
257 postsynaptic dendritic arbors.

258



259  
 260 **Figure 3: DJ-1 $\beta$  senses ROS and regulates activity-induced neural plasticity.** (A) DJ-1 $\beta$  is required for  
 261 ROS and neuronal-activity-induced NMJ elaboration (100hrs ALH). Larvae reared at 25°C. (B) Cell-  
 262 specific expression of DJ-1 $\beta^{C104A}$ , non-oxidizable on conserved cysteine C104, prevents activity-  
 263 induced reduction of active zone number. ‘Control’ is aCC/RP2-GAL4 alone. Larvae were reared at  
 264 25°C. (C) Activity-generated ROS sensing is dose sensitive. Removal of one copy of DJ-1 $\beta$  (in DJ-1 $\beta^{A93}$  /  
 265 + heterozygotes) is sufficient to significantly rescue activity-induced reduction of total dendritic arbor  
 266 length of motoneurons in 24hr ALH larvae. ‘Control’ is aCC-FLP-GAL4 alone, heterozygous, achieved  
 267 by crossing the GAL4 driver to Oregon-R wild type flies.

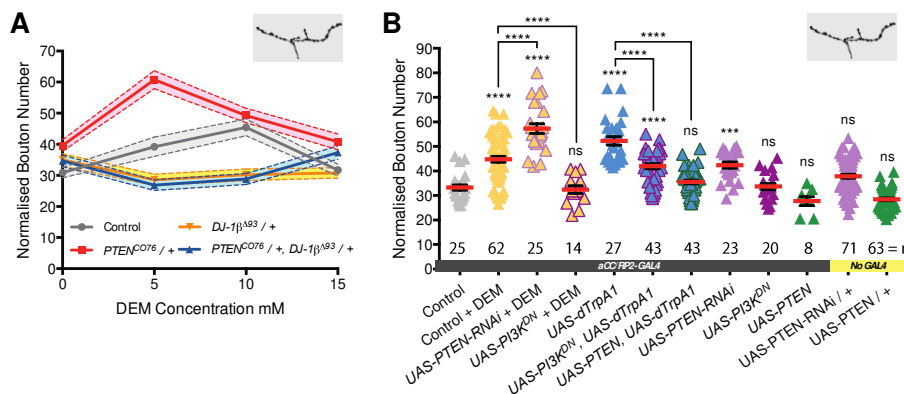
268  
 269

### 270 PTEN and PI3K are downstream effectors of the DJ-1 $\beta$ ROS sensor

271 Next, we looked for downstream effector pathways responsible for implementing activity and ROS-  
 272 dependent structural plasticity. DJ-1 is a known redox-regulated inhibitor of PTEN and as such  
 273 disinhibits PI3Kinase signaling (Kim et al., 2005; Kim et al., 2009b). PI3Kinase was previously shown  
 274 to regulate bouton and active zone number during NMJ development (Jordán-Álvarez et al., 2012;  
 275 Martín-Peña et al., 2006). To test if DJ-1 $\beta$  - PTEN interactions mediate ROS-dependent NMJ  
 276 adjustments, we performed genetic interaction experiments in the context of DEM-induced ROS  
 277 elevation (Milton et al., 2011) (Figure 4A). We used different DEM dosages to generate a dose-  
 278 response curve and focused on changes in NMJ bouton number as a quantitative readout. We found  
 279 that in controls bouton number increases linearly with exposure to increasing DEM concentrations,  
 280 peaking at 15mM DEM (Figure 4A). Removal of one copy of DJ-1 $\beta$  (DJ-1 $\beta^{A93}$  / +) was sufficient to  
 281 suppress these DEM-induced increases in bouton number. Conversely, removing one copy of the

282 PI3Kinase antagonist PTEN ( $PTEN^{CO76}/+$ ) resulted in increased sensitivity to DEM, as indicated by the  
 283 left-shifted dose response curve. Larvae made heterozygous mutant for both  $DJ-1\beta$  and  $PTEN$   
 284 ( $PTEN^{CO76}/+; DJ-1\beta^{\Delta93}/+$ ) were overall less sensitive to DEM than controls, though at higher  
 285 concentrations displayed greater sensitivity to DEM than  $DJ-1\beta^{\Delta93}/+$  heterozygotes, as might be  
 286 expected when lowering  $PTEN$  copy number. These genetic interactions support previous studies  
 287 (Kim et al., 2005) and complement biochemical data that showed increased binding of  $DJ-1\beta$  to  $PTEN$   
 288 following oxidation by  $H_2O_2$ , thus effecting  $PTEN$  inhibition (Kim et al., 2009b).

289 To further test specificity, we manipulated  $PTEN$  and PI3Kinase activities in single cells.  
 290 Targeted knock-down of endogenous  $PTEN$  in aCC and RP2 motoneurons sensitized these to ROS,  
 291 exacerbating the DEM-induced bouton addition phenotype (Figure 4B). In contrast, over-expression  
 292 of  $PTEN$  or mis-expression of a dominant negative form of PI3Kinase significantly reduced NMJ  
 293 elaboration normally caused by DEM exposure or dTrpA1-mediated overactivation (Figure 4B).  
 294 Together these genetic interactions suggest a working model whereby  $PTEN$  and PI3Kinase act  
 295 downstream of  $DJ-1\beta$ ; and neural activity-generated ROS, via oxidation of  $DJ-1\beta$ , leads to  $PTEN$   
 296 inhibition. This in turn facilitates a rise in PI3Kinase /  $PIP_3$  signaling, which mediates at least part of  
 297 the structural synaptic terminal plasticity by regulating bouton and active zone number at the NMJ  
 298 (Figure 7).



299 **Figure 4:  $DJ-1\beta$  signals via  $PTEN$  and PI3Kinase to regulate ROS and activity-induced NMJ**  
 300 **elaboration.** (A)  $DJ-1\beta$  and  $PTEN$  genetically interact to regulate systemic ROS-induced NMJ  
 301 elaboration. NMJ bouton number varies with ROS (DEM) levels (grey data). Removal of one copy of  
 302  $PTEN$  sensitizes (red) while heterozygosity for  $DJ-1\beta$  desensitizes NMJs to ROS levels (yellow), partially  
 303 restored in double heterozygotes (blue). Dashed boundaries indicate 95 % confidence intervals  
 304 ( $n \geq 38$ ). (B) Systemic ROS and activity-induced NMJ structural adjustments require  $PTEN$  and  
 305 PI3Kinase signaling. Over-expression of the PI3Kinase antagonist  $PTEN$  or a dominant negative  
 306 PI3Kinase form abrogates activity-induced NMJ elaboration. 'Control' is aCC/RP2-GAL4 alone,  
 307 heterozygous, achieved by crossing the GAL4 driver to Oregon-R wild type flies. Mean  $\pm$  SEM,  
 308 ANOVA, ns = not significant, \*\* $P < 0.01$ , \*\*\* $P < 0.001$ , \*\*\*\* $P < 0.0001$ , n = replicate number.

310

311

### 312 Activity-regulated ROS signaling is necessary for homeostatic adjustment of synaptic 313 transmission at the NMJ

314 To complement our studies of structural plasticity at the NMJ, we carried out sharp electrode  
 315 recordings from the target muscle co-innervated by the aCC and RP2 motoneurons, muscle dorsal

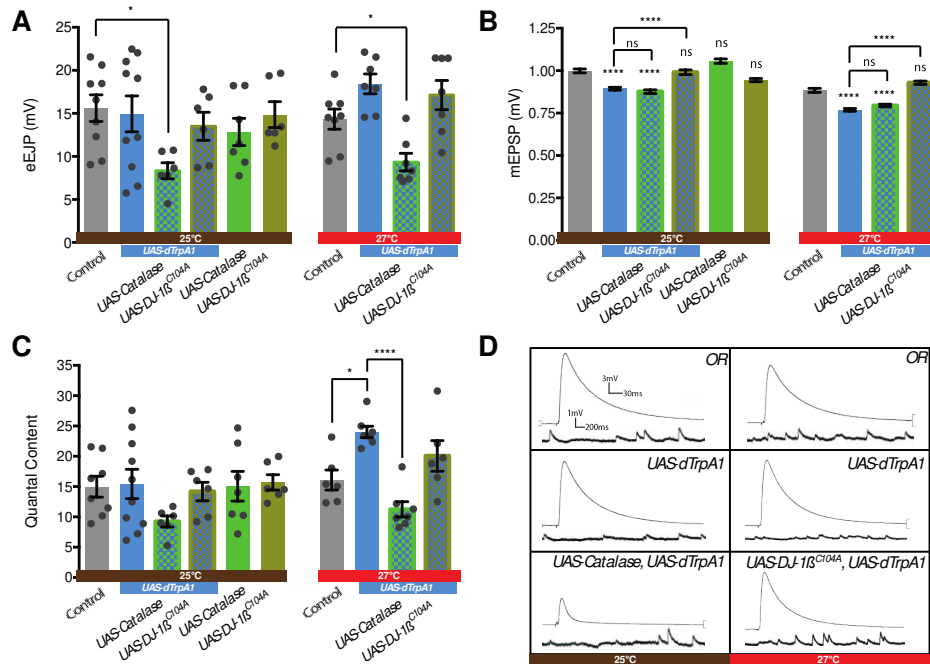
316 acute 1 (DA1) (Hoang and Chiba, 2001; Landgraf et al., 2003; Mauss et al., 2009). In Oregon-R wild  
317 type larvae we recorded evoked excitatory junction potentials (eEJPs) of  $18 \pm 2$ mV (Figure 5A, D) and  
318 miniature excitatory junction potentials (mEJPs) indicative of spontaneous vesicle fusion of 1mV  
319 (Figure 5B, D). Therefore, on average each action potential triggers fusion of 18 vesicles at this NMJ  
320 (quantal content) (Figure 5C).

321 We investigated how these parameters of NMJ transmission might change following cell-  
322 specific dTrpA1-mediated overactivation of the aCC and RP2 motoneurons (at 25°C and 27°C). We  
323 then tested if these activity-driven changes in transmission required ROS signaling, by co-expressing  
324 the ROS scavenger Catalase or by abrogating ROS sensor function through co-expression of the  
325 dominant acting, non-oxidizable DJ-1 $\beta$  variant, DJ-1 $\beta^{C104A}$ . Transmission at NMJs in *Drosophila* is  
326 characteristically robust due to several homeostatic regulatory mechanisms working toward  
327 maintaining constancy of eEJPs (for reviews see (Frank, 2014; Frank et al., 2013; Harris and Littleton,  
328 2015)). Following dTrpA1-mediated overactivation (rearing larvae at 25°C and 27°C) evoked NMJ  
329 transmission at the muscle DA1 NMJ remains intact and homeostatically balanced (Figure 5A, D).  
330 Recordings from controls and larvae with dTrpA1 expressing motoneurons reared at 27°C showed  
331 noticeably less variability of eEJP amplitude than those made from genetically identical siblings  
332 reared at 25°C, the dTrpA1 activation threshold, potentially reflecting variable efficacy in  
333 motoneuron manipulation (Hamada et al., 2008; Pulver et al., 2009). Overexpression of either  
334 Catalase or DJ-1 $\beta^{C104A}$  has no effect on eEJP amplitude. However, co-expression of Catalase with  
335 dTrpA1-mediated overactivation leads to reduction of eEJP amplitude to 7-9mV. This suggests that  
336 ROS are required for mechanisms that homeostatically maintain eEJP amplitude (Figure 5A, D).

337 In contrast, the amplitude of spontaneous vesicle fusion events (mEJP) adjusts inversely with  
338 progressively stronger overactivation of motoneurons. These reductions in mEJP amplitude are not  
339 specific to dTrpA1-mediated overactivation. Along with others (Ueda and Wu, 2015; Yeates et al.,  
340 2017) we also recorded similarly reduced mEJP amplitudes in wild type Oregon-R larvae that had  
341 been reared at an elevated temperature (27°C *versus* controls reared at 25°C) (Figure 5B). Co-  
342 expression of DJ-1 $\beta^{C104A}$  abrogates this activity-dependent reduction of mEJP amplitude (Figure 5B,  
343 D), while Catalase co-expression has no effect on mEJP amplitude. Our analysis of quantal content  
344 (the mean number of vesicles releasing transmitter per action potential, calculated as the ratio of  
345 eEJP/mEJP amplitudes) showed that dTrpA1-mediated motoneuron over-activation at 27 °C leads to  
346 significantly increased quantal content, and that this is brought back to control levels with co-  
347 expression of the H<sub>2</sub>O<sub>2</sub> scavenger Catalase, as might be expected from the reduced eEJP amplitudes  
348 under such conditions.

349 In summary, evoked transmission at the NMJ is homeostatically maintained despite  
350 increased dTrpA1-mediated neuronal overactivation. The maintenance of eEJP amplitude requires  
351 ROS and is compromised when the H<sub>2</sub>O<sub>2</sub> scavenger Catalase is expressed by the presynaptic  
352 motoneuron. Activity-regulated changes in mEJP amplitude also depend on ROS signaling, though  
353 this is not impacted by the over-expression of cytoplasmic Catalase; instead we found this aspect of  
354 synaptic transmission sensitive to oxidation of DJ-1 $\beta$ .

355



356

357

358

359

360

361

362

363

364

365

366

367

368

369

370

371

372

373

374

375

376

377

378

379

380

381

382

**Figure 5: Pre-synaptic ROS regulate the maintenance of eEJP amplitude and DJ-1 $\beta$  function is required for the reduction of mEJP amplitude during overactivation.** (A) Overactivated motoneurons (expressing dTrpA1 at 25°C, 27°C) show similar eEJP amplitude to control, despite reduced mEJP amplitude (see B). Catalase co-expression prevents this adaptation, significantly reducing eEJP amplitude, whereas DJ-1 $\beta$  appears not to be required. (B) Increased neuronal activity, mediated by dTrpA1 expression at 25°C or by elevating ambient temperature to 27°C, reduces mEJP amplitude. Co-expression of DJ-1 $\beta^{C104A}$  rescues this effect. (C) Quantal content (eEJP amplitude / mEJP amplitude) shows no significant difference between groups due to high variance within some conditions. (D) Representative eEJP and mEJP traces. ANOVA, ns = not significant, \*  $P < 0.05$ , \*\*\*\*  $P < 0.0001$ .

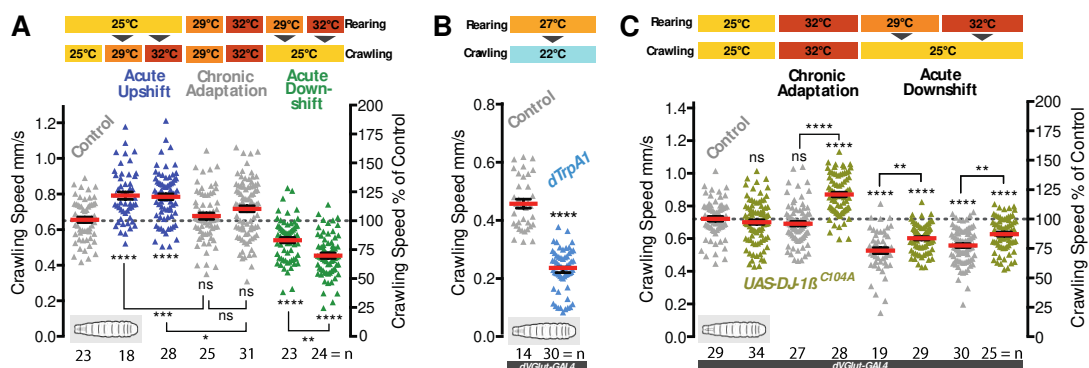
### Structural plasticity of synaptic terminals is required for homeostatic adjustment of locomotor behavior

We wondered what impact the observed activity-ROS-regulated structural adjustments might have on network output. To test this we used larval crawling speed as a quantifiable readout for a simple locomotor behavior. In agreement with a previous study (Sigrist et al., 2003; Zhong and Wu, 2004), we found that crawling speed increases upon acutely shifting mid-3<sup>rd</sup> instar larvae (72 hours ALH) to higher ambient temperatures (e.g., from 25°C to 29°C or 32°C) (blue data in Figure 6A). This is to be expected given that these animals have an innate preference for approximately 25°C (Dillon et al., 2009; Hamada et al., 2008; Luo et al., 2016; Rosenzweig et al., 2005). In contrast, following prolonged exposure to an elevated temperature, achieved by rearing larvae at 29°C or 32°C, larvae crawled at the same speed characteristic of controls reared at 25°C (average of 0.65 – 0.72mm/second; grey horizontal dotted line in Figure 6A). This crawling speed adaptation is suggestive of a homeostatic adjustment of the locomotor network. Increased network drive might be counteracted by reduced neuronal excitability and/or synaptic input, thus allowing motor output

383 to be returned to the default crawling speed; in which case one would expect greater adjustment in  
 384 larvae reared at 32°C than 29°C. To reveal such adjustments we acutely shifted warmth-adapted  
 385 animals to 25°C, which caused reduced crawling speed (green data in Figure 6A). Indeed, following  
 386 this downward-shift 32°C-adjusted larvae crawled significantly slower than 29°C-adjusted animals,  
 387 suggesting the degree of neuronal adjustment is proportional to the level of temperature-induced  
 388 overactivation. These experiments suggest that during prolonged activity manipulations the larval  
 389 locomotor network output homeostatically adjusts toward a default crawling speed.

390 Next, we wanted to test the role of the motoneurons in this form of network adjustment.  
 391 The motoneurons integrate all pre-motor input within their dendritic arbors and produce the output  
 392 of the motor network. We targeted expression of dTrpA1 to the motoneurons (and other  
 393 glutamatergic cells, using *DvGlut-T2A-GAL4*) and reared these animals at 27°C, a temperature that  
 394 robustly activates dTrpA1-expressing neurons (Hamada et al., 2008; Pulver et al., 2009). Upon acute  
 395 removal of this overstimulation (by shifting animals to 22°C where the dTrpA1 channel is closed)  
 396 larval crawling speed reduced significantly relative to non-dTrpA1 expressing controls (Figure 6B).  
 397 We then asked whether this ROS-mediated structural plasticity of synaptic terminal growth was  
 398 required for homeostatic adjustment of larval crawling speed, which ensues after prolonged  
 399 overactivation. We manipulated the ability of neurons to sense increases in ROS levels by targeting  
 400 expression of the dominant acting non-oxidizable DJ-1 $\beta^{C104A}$  variant to motoneurons. We then tested  
 401 the behavior of these animals for adjustment in response to chronic temperature-induced elevation  
 402 of motor network activity. Our previous set of experiments showed that expression of non-  
 403 oxidizable DJ-1 $\beta^{C104A}$  in motoneurons prevents structural adjustment of bouton number and the  
 404 decrease in active zone number normally caused by overactivation (see Figures 3A & 3B). Expression  
 405 of non-oxidizable DJ-1 $\beta^{C104A}$  in motoneurons *per se* did not alter larval crawling speed at the control  
 406 temperature of 25°C. However, when rearing these larvae at 32°C, which is associated with elevated  
 407 motor network activation, unlike controls they failed to homeostatically adjust toward the default  
 408 crawling speed (Figure 6C). Consequently, such larvae reared at elevated temperatures (29°C or  
 409 32°C) also responded less strongly than controls to acute temperature downshifts (Figure 6C). These  
 410 data suggest that activity-induced structural plasticity, implemented through the ROS sensor DJ-1 $\beta$ ,  
 411 is necessary for activity-directed homeostatic adjustment of larval locomotor behavior.

412

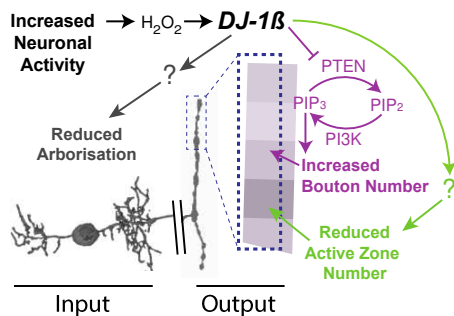


413

414

415 **Figure 6: Adaptive behavioral plasticity in response to chronic locomotor overactivation.** (A)  
 416 Larval motor network activity, assayed by crawling speed 72hrs after larval hatching (AHL), increases

417 in response to acute temperature upshifts (blue) in wild type larvae. In contrast, with prolonged  
 418 exposure (grey) to elevated temperatures (29°C or 32°C) the motor network adapts homeostatically  
 419 generating the same crawling speed as 25°C reared controls. This adaptation is further revealed by  
 420 acute temperature downshifts (green). Each data point represents crawling speed from an individual  
 421 uninterrupted continuous forward crawl,  $n$  = specimen replicate number, up to 3 crawls assayed for  
 422 each larva. Genotype = OregonR. (B) Prolonged overactivation targeted to motoneurons (dVGlut-  
 423 GAL4; UAS-dTrpA1) also leads to adaptation with reduced crawling speed (dTRPA1 channels open at  
 424 27°C, closed at 22°C). Mean +/- SEM, control is dVGlut-GAL4 / +. \*\*\*\* $P < 0.0001$  students  $t$  test,  $n$  =  
 425 replicate number. (C) Larvae with expression of UAS-DJ-1 $\beta^{C104A}$  targeted to motoneurons (dVGlut-  
 426 GAL4) are unable to adapt motor network output (crawling speed) to elevated rearing temperatures.  
 427 Control is dVGlut-GAL4 alone, in heterozygous condition. Each data point represents crawling speed  
 428 from an individual uninterrupted continuous forward crawl,  $n$  = specimen replicate number, up to 3  
 429 crawls assayed for each larva. Mean +/- SEM, ANOVA, ns = not significant, \* $P < 0.05$ , \*\* $P < 0.01$ ,  
 430 \*\*\* $P < 0.001$ , \*\*\*\* $P < 0.0001$ .



432  
 433

434 **Figure 7: Model summary.** DJ-1 $\beta$  is a redox signaling hub that coordinates structural synaptic  
 435 plasticity at motoneuron synaptic input and output terminals. Activity-induced ROS oxidize DJ-1 $\beta$ ,  
 436 leading to PTEN inhibition and thus to a gain in PI3Kinase signaling, which regulates activity-induced  
 437 NMJ elaboration of boutons and active zones. At higher activity/ROS thresholds additional, yet to be  
 438 defined, pathways downstream of DJ-1 $\beta$  are activated, implementing adaptive reductions of active  
 439 zones at the NMJ and dendritic arbor length in the CNS.

440  
 441

## 442 Discussion

443

### 444 ROS signaling is required for neuronal activity-dependent structural plasticity

445 Building on previous work that had shown oxidative stress as inducing NMJ growth (Milton et al.,  
 446 2011), we have in this study identified ROS as obligatory signals for activity-regulated structural  
 447 plasticity. We further show that ROS are also sufficient to bring about structural changes at synaptic  
 448 terminals that largely mimic those induced by neuronal overactivation (Figure 2B, C). A  
 449 mitochondrially targeted ROS reporter (Albrecht et al., 2011; Gutscher et al., 2009) suggests a  
 450 positive correlation between levels of neuronal activity and ROS generated in mitochondria,  
 451 potentially as a byproduct of increased ATP metabolism or triggered by mitochondrial calcium influx

452 (Peng and Jou, 2010) (Figure 2A). Although we did not specifically investigate the nature of the  
453 active ROS in this context, three lines of evidence suggest that H<sub>2</sub>O<sub>2</sub>, generated by the dismutation of  
454 O<sub>2</sub><sup>-</sup>, is the principal signaling species. First, under conditions of neuronal overactivation (but not  
455 control levels of activity) over-expression of the O<sub>2</sub><sup>-</sup> to H<sub>2</sub>O<sub>2</sub> converting enzyme SOD2 potentiated  
456 structural plasticity phenotypes (Figure 2B). Second, over-expression of the H<sub>2</sub>O<sub>2</sub> scavenger Catalase  
457 efficiently counter-acts all activity-induced changes we have quantified, at both postsynaptic  
458 dendritic and presynaptic NMJ terminals. Third, over-expression of the H<sub>2</sub>O<sub>2</sub> generator Duox in  
459 motoneurons is sufficient to induce NMJ bouton phenotypes that mimic overactivation (Figure 3A).  
460 In addition to mitochondria, other sources of ROS include several oxidases, notably NADPH oxidases.  
461 These have been implicated during nervous system development in the regulation of axon growth  
462 and synaptic plasticity (Kishida et al., 2006; Munnamalai and Suter, 2009; Munnamalai et al., 2014;  
463 Olguin-Albuerne and Morán, 2015; Serrano et al., 2003; Tejada-Simon et al., 2005; Wilson et al.,  
464 2016; Wilson et al., 2015). NADPH oxidases can be regulated by NMDA receptor stimulation  
465 (Brennan et al., 2009) and activity-associated pathways, including calcium, Protein kinases C and A  
466 and calcium/calmodulin-dependent kinase II (CamKII) (Bánfi et al., 2004; Massaad and Klann, 2011;  
467 Pandey et al., 2011; Sorce et al., 2017; Tirone and Cox, 2007). The precise sources of activity-  
468 regulated ROS, potentially for distinct roles in plasticity, will be interesting to investigate.

469

#### 470 **ROS as gatekeepers of activity-dependent synaptic structural plasticity**

471 We demonstrated that ROS are necessary for activity-dependent structural plasticity of *Drosophila*  
472 motoneurons, at both their postsynaptic dendrites in the CNS and presynaptic NMJs in the  
473 periphery. The mechanisms by which ROS intersect with other known plasticity pathways now need  
474 to be investigated. Among well documented signaling pathways regulating synaptic plasticity, are  
475 Wnts (Budnik and Salinas, 2011), BMPs (Bayat et al., 2011; Berke et al., 2013), PKA, CREB and the  
476 immediate early gene transcription factor AP-1 (Cho et al., 2015; Davis, 2006; Davis and Müller,  
477 2015; Davis et al., 1998; Davis et al., 1996; Kim et al., 2009a; Koles and Budnik, 2012; Osses and  
478 Henriquez, 2014; Sanyal et al., 2003; Sanyal et al., 2002; Sulkowski et al., 2014; Walker et al., 2013).  
479 ROS signaling could be synergistic with other neuronal plasticity pathways, potentially integrating  
480 metabolic feedback. Indeed, ROS modulate BMP signaling in cultured sympathetic neurons  
481 (Chandrasekaran et al., 2015) and Wnt pathways in non-neuronal cells (Funato et al., 2006; Love et  
482 al., 2013; Rharass et al., 2014). Biochemically, ROS are well known regulators of kinase pathways via  
483 oxidation-mediated inhibition of phosphatases (Finkel and Holbrook, 2000; Tonks, 2006). Redox  
484 modifications also regulate the activity of the immediate early genes Jun and Fos, which are required  
485 for LTP in vertebrates, and in *Drosophila* for activity-dependent plasticity of motoneurons, both at  
486 the NMJ and central dendrites (Hartwig et al., 2008; Jindra et al., 2004; Loebrich and Nedivi, 2009;  
487 Milton and Sweeney, 2012; Milton et al., 2011; Sanyal et al., 2002). We therefore hypothesize that  
488 ROS may provide neuronal activity-regulated modulation of multiple canonical synaptic plasticity  
489 pathways.

490

#### 491 **Structural plasticity and its coordination between pre- and postsynaptic terminals**

492 We focused on three aspects of synaptic terminal plasticity: dendritic arbor size in the CNS, and  
493 bouton and active zone numbers at the NMJ. We used these as phenotypic indicators for activity-  
494 regulated changes. By working with identified motoneurons we could observe adaptations across

495 the entire neuron, relating adjustments of postsynaptic dendritic input terminals in the CNS to  
496 changes of the presynaptic output terminals at the NMJ in the periphery. For the aCC motoneuron,  
497 the degree of neuronal overactivation correlates with changes in synaptic terminal growth: notably  
498 reductions of dendritic arbor size centrally and of active zones at the NMJ. Interestingly, presynaptic  
499 active zone numbers did not show a linear response profile. Within a certain range low-level activity  
500 increases lead to more active zones, associated with potentiation (as previously shown (Sigrist et al.,  
501 2003)); however, with stronger overactivation active zone number decrease (Figure 1D, E).  
502 Reduction of active zones, as we observed at the NMJ, and of Brp levels by increased activation was  
503 previously also reported in photoreceptor terminals of the *Drosophila* adult visual system (Sugie et  
504 al., 2015). At a finer level of resolution it will be interesting to determine how these activity-ROS-  
505 mediated structural changes might change active zone cytomatrix composition, which can impact on  
506 transmission properties, such as vesicle release probability (Davydova et al., 2014; Lazarevic et al.,  
507 2011; Matz et al., 2010; Peled et al., 2014; Weyhersmüller et al., 2011)

508 We previously found that in these motoneurons dendritic length correlates with the number  
509 of input synapses and with synaptic drive (Zwart et al., 2013). Therefore, we tentatively interpret the  
510 negative correlation between the degree of overactivation and the reduction in central dendritic  
511 arbors as compensatory. In agreement, we found that blockade of activity-induced structural  
512 adjustment targeted to the motoneurons prevents behavioral adaptation normally seen after  
513 prolonged overactivation (Figure 6). Less clear is if and how overactivation-induced structural  
514 changes at the NMJ might be adaptive. Unlike many central synapses that facilitate graded analogue  
515 computation, the NMJ is a highly specialized synapse with a large safety factor and intricate  
516 mechanisms that ensure constancy of evoked transmission in essentially digital format (Frank et al.,  
517 2013; Marrus and DiAntonio, 2005). Rearing larvae at 29°C (which acutely increases motor activity)  
518 leads to more active zones at the NMJ and potentiated transmission, yet these larvae crawl at the  
519 same default speed as other larvae reared at 25°C (control) or 32°C with reduced numbers of active  
520 zones (compare Figure 1E with Figure 6B). This suggests that at least with regard to regulating  
521 crawling speed, plasticity mechanisms probably operate at the network level, rather than  
522 transmission properties of the NMJ. Indeed, our recordings of transmission at the NMJ, and those  
523 reported by others, show homeostatic maintenance of eEJP amplitude irrespective of changes in  
524 bouton and active zone number (Figure 5) (Campbell and Ganetzky, 2012). Though in this study we  
525 focused on anatomical changes, we expect these structural adjustments to be linked to, and  
526 probably preceded by compensatory changes in neuronal excitability that have been documented  
527 (Baines et al., 2001; Davis, 2006; Davis et al., 1996; Davis et al., 1998; Driscoll et al., 2013; Frank et  
528 al., 2006; Frank et al., 2009; Gaviño et al., 2015; Giachello and Baines, 2016; Lin et al., 2012b; Mee et  
529 al., 2004; Müller and Davis, 2012; Wang et al., 2014; Younger et al., 2013; O'Leary et al., 2013; Prinz,  
530 2006; Prinz et al., 2004).

531 Our observations of activity-regulated adjustments of both dendritic arbor size and NMJ  
532 structure give the impression of processes coordinated across the entire neuron. If this was the case,  
533 it could be mediated by transcriptional changes, potentially via immediate early genes (AP-1), which  
534 are involved in activity and ROS-induced structural changes at the NMJ (Milton et al., 2011; Sanyal et  
535 al., 2002) and motoneuron dendrites (Hartwig et al., 2008).

536  
537

## 538 **Identification of DJ-1 $\beta$ as a neuronal ROS sensor**

539 We discovered that in neurons the highly conserved protein DJ-1 $\beta$  is critical for both  
540 structural and physiological changes in response to activity-generated ROS (Figure 3 and Figure 5). In  
541 neurons DJ-1 $\beta$  might act as a redox sensor for activity-generated ROS. In agreement with this idea,  
542 DJ-1 $\beta$  has been shown to be oxidized by H<sub>2</sub>O<sub>2</sub> at the conserved cysteine residue C106 (C104 in  
543 *Drosophila*) (Lin et al., 2012a; Meulener et al., 2006). Oxidation of DJ-1 leads to changes in DJ-1  
544 function, including translocation from the cytoplasm to the mitochondrial matrix, aiding protection  
545 against oxidative damage (Blackinton et al., 2009; Canet-Avilés and Wilson, 2004; Waak et al., 2009)  
546 and maintenance of ATP levels (Calì et al., 2015). We found that the ability of motoneurons to  
547 respond to increased activation is potently sensitive to DJ-1 $\beta$  dosage. It is also blocked by expression  
548 of mutant DJ-1 $\beta$ <sup>C104A</sup> that is non-oxidisable on the conserved Cys104 (Hao et al., 2010; Meulener et  
549 al., 2006). These observations suggest that DJ-1 $\beta$  is critical to ROS sensing in neurons. They also  
550 predict that cell type-specific DJ-1 $\beta$  levels, and associated DJ-1 $\beta$  reducing mechanisms, could  
551 contribute to setting cell type-specific sensitivity thresholds to neuronal activity.

552

553

554

555

## 556 **DJ-1 $\beta$ downstream pathways implement activity-regulated plasticity**

557 Our data suggest that DJ-1 $\beta$  could potentially be part of a signaling hub. At the NMJ, this might  
558 mediate plasticity across a range, from the addition of active zones associated with potentiation to,  
559 following stronger overactivation, the reduction of active zones. We identified disinhibition of  
560 PI3Kinase signaling as one DJ-1 $\beta$  downstream pathway (Figure 4) (Kim et al., 2005; Kim et al., 2009b),  
561 a well-studied intermediate in metabolic pathways and a known regulator of synaptic terminal  
562 growth, including active zone addition (Jordán-Álvarez et al., 2012; Martín-Peña et al., 2006).  
563 However, with stronger overactivation DJ-1 $\beta$  might engage additional downstream effectors that  
564 reduce active zone addition or maintenance, potentially promoting active zone disassembly. While  
565 at the presynaptic NMJ PI3Kinase disinhibition explains activity-regulated changes in bouton  
566 addition, different DJ-1 $\beta$  effectors likely operate in the somato-dendritic compartment, which  
567 responds to overactivation with reduced growth and possibly pruning (Brierley et al., 2009). Thus,  
568 sub-cellular compartmentalization of the activity-ROS-DJ-1 $\beta$  signaling axis could produce distinct  
569 plasticity responses in pre- *versus* postsynaptic terminals.

570

571

## 572 **Homeostatic maintenance of synaptic transmission requires presynaptic ROS signaling**

573 Previous studies demonstrated a requirement for ROS for LTP (Huddleston et al., 2008; Kamsler and  
574 Segal, 2003a; Kamsler and Segal, 2003b; Klann, 1998; Knapp and Klann, 2002; Lee et al., 2010) and  
575 found learning defects in animal models with reduced NADPH oxidase activity (Kishida et al., 2006),  
576 suggesting that synaptic ROS signaling might be a conserved feature of communication in the  
577 nervous system. Our sharp electrode recordings from muscle DA1 revealed three interesting  
578 aspects. First, that changing ROS signaling in the presynaptic motoneuron under normal activity  
579 conditions does not obviously impact on NMJ transmission. Second, quenching of presynaptic ROS  
580 by expression of Catalase under overactivation conditions led to a significant decrease in eEJP

581 amplitude and concomitantly reduced quantal content (Figure 5A, C). This shows that upon chronic  
582 neuronal overactivation ROS signaling is critically required in the presynaptic motoneuron for  
583 maintaining eEJP amplitude by increasing vesicle release at the NMJ. This could be achieved by  
584 increasing vesicle release probability, which would counteract the reduction in active zone number  
585 following a period of neuronal overactivation. In this context it is interesting that components of the  
586 presynaptic release machinery, including SNAP25, are thought to be directly modulated by ROS  
587 (Giniatullin et al., 2006), while others, such as Complexin, might be indirectly affected, e.g., via ROS-  
588 mediated inhibition of phosphatases leading disinhibition of kinase activity (Cho et al., 2015). Third,  
589 we found that overactivation of motoneurons leads to reduced mEJP amplitude, also recently  
590 reported by others (Yeates et al., 2017). Curiously, mEJP amplitude, unlike eEJP amplitude, is  
591 regulated by DJ-1 $\beta$ , but is not impacted on by artificially increased cytoplasmic levels of the H<sub>2</sub>O<sub>2</sub>  
592 scavenger Catalase. How it is that under conditions of neuronal overactivation eEJP and mEJP  
593 amplitudes are differentially sensitive to cytoplasmic Catalase *versus* DJ-1 $\beta$  oxidation is unclear,  
594 though it marks these two processes as distinct. One possibility is that cytoplasmic Catalase changes  
595 the local redox status, which could directly affect the properties of the presynaptic active zone  
596 cytomatrix. In contrast, mEJP amplitude regulation might be indirect and cell non-autonomous, via  
597 modulation of glutamate receptors in the postsynaptic target muscle (Davis et al., 1998).  
598 Furthermore, these ROS-regulated adjustments in synaptic transmission are at

599         Thus, several distinct ROS responsive pathways appear to operate at the NMJ. Structural  
600 adjustments in terms of synaptic terminal growth and synapse number are mediated by mechanisms  
601 sensitive to DJ-1 $\beta$  oxidation, potentially regulated via local reducing systems, including Catalase. In  
602 addition and distinct from these structural changes, at least in part, are the ROS-regulated  
603 adjustments in synaptic transmission that show different ROS sensitivities, one maintaining quantal  
604 content of evoked transmission while the other reduces mEJP amplitude when neuronal activity  
605 goes up (Figure 5B). It is conceivable that spatially distinct sources of ROS, e.g. mitochondria *versus*  
606 membrane localized NADPH oxidases, with different temporal dynamics could potentially mediate  
607 such differences in ROS sensitivities at the NMJ.

608

### 609 **Homeostatic adjustment of larval crawling speed depends on redox modification of DJ-1 $\beta$**

610 Our experiments exploring the potential behavioral relevance of activity-regulated structural  
611 plasticity demonstrated that network drive is regulated by ambient temperature. Acute elevation in  
612 ambient temperature produces faster crawling, while acute temperature reductions have the  
613 opposite effect. In contrast, with chronic temperature manipulations, larval crawling returns to its  
614 default speed (approx. 0.65 – 0.72mm/sec) (Figure 6A). This adaptation to chronic manipulations  
615 might overall be energetically more favorable. It also allows larvae to retain a dynamic range of  
616 responses to relative changes in ambient temperature (i.e. speeding up or slowing down).

617         Where in the locomotor network these adjustments take place remains to be worked out. It  
618 is reasonable to assume that proprioceptive sensory neurons, and potentially also central recurrent  
619 connections, provide feedback information that facilitates homeostatic adjustment of network  
620 output. Our manipulations of the glutamatergic motoneurons show these cells are clearly important.  
621 For example, cell type-specific overactivation of the glutamatergic motoneurons (via dTrpA1) on the  
622 one hand, and blockade of activity-induced structural adjustment (by mis-expression of non-  
623 oxidizable DJ-1 $\beta$ <sup>C104A</sup>) on the other demonstrated that ROS-DJ-1 $\beta$ -mediated processes that we

624 showed important for structural adjustment are also required for implementing homeostatic tuning  
625 of locomotor network output (Figure 6B, C). The capacity of motoneurons as important elements in  
626 shaping motor network output, might be explicable in that these neurons constitute the final  
627 integrators on which all pre-motor inputs converge (Fushiki et al., 2016; Itakura et al., 2015; Kohsaka  
628 et al., 2014; Schneider-Mizell et al., 2016; Zwart et al., 2016).

629

630 In conclusion, here we identified ROS in neurons as novel signals that are critical for activity-induced  
631 structural plasticity. ROS levels regulated by neuronal activity have the potential for operating as  
632 metabolic feedback signals. We further identified the conserved redox-sensitive protein DJ-1 $\beta$  as  
633 important to neuronal ROS sensing, and the PTEN/PI3Kinase synaptic growth pathway as a  
634 downstream effector pathway for NMJ growth in response to neuronal overactivation. These  
635 findings suggest that in the nervous system ROS operate as feedback signals that inform cells about  
636 their activity levels. The observation that ROS are important signals for homeostatic processes  
637 explains why ROS buffering is comparatively low in neurons (Bell et al., 2015). This view also shines a  
638 new light on the potential impact of ROS dysregulation with age or under neurodegenerative  
639 conditions, potentially interfering with neuronal adaptive adjustments and thereby contributing to  
640 network malfunction and synapse loss.

641

642

643

644 **Competing interests:** The authors declare that no competing interests exist.

645

646

647

648

649

650 **Acknowledgements:**

651

652 We would like to thank Richard Ribchester for invaluable help with setting up a rig for NMJ sharp  
653 electrode recording. Nancy Bonini, Tobias Dick, Jörg Grosshans, Karen Hibbard, Fanis Missirlis, Barret  
654 Peiffer and Alex Whitworth for generous reagent donations, and Akinao Nose and Hiroshi Kohsaka  
655 for kindly helping with figure 1. We would also like to thank Jimena Berni, Alex Whitworth and  
656 members of the Landgraf lab for valuable comments on the manuscript. This work was supported by  
657 BBSRC research grants (BB/IO1179X/1, BB/M002934/1) to ML and (BB/IO12273/1, BB/M002322/1)  
658 to STS.

659

660

661 **Materials and Methods**

662

663 **Electrophysiology.** Late wandering third instar larvae were fillet dissected in standard HL3 buffer  
664 (adapted from (Stewart et al., 1994), 70mM NaCl, 5mM KCl, 20mM MgCl<sub>2</sub>, 10mM NaHCO<sub>3</sub>, 115mM  
665 Sucrose, 5mM HEPES, 1.5mM CaCl, pH 7.25) ventral surface down with a lateral incision in order  
666 preserve both the ventral and dorsal midlines. Suction (GC150F-10 Harvard Apparatus) and sharp

667 (GC100F-10 Harvard Apparatus) electrodes were pulled using a P-97 pipette puller (Sutter  
668 Instrument Company). Sharp electrode muscle impalement (DA1 muscle, at the dorsal midline) and  
669 inter-segmental nerve suction (ventral midline) were performed using an Olympus BX50WI  
670 compound microscope with 10X air (Olympus 10x/0.25) and 20X dipping (Olympus UMPIanFL  
671 20x/0.5w) objective lenses. Recordings were made at 21°C in HL3 using an Axopatch-1D amplifier  
672 (Axon Instruments), a 1322A DigiData (Axon Instruments), a DS2A-MkII Constant Voltage Isolated  
673 Stimulator (Digitimer Ltd.) and pCLAMP 10.4 acquisition software (Molecular Devices). mEJP (2-  
674 3minutes) and eEJP (3 rounds of 20 stimulations, 5V) recordings were made in current-clamp mode  
675 from muscle cells with an input resistance above 8MOhm and a stable resting membrane potential  
676 between -40mV and -70mV. Analysis of eEJPs was performed using Clampfit10.6 (Molecular  
677 Devices) and mEJPs using Mini-Analysis6.0.7 (Synaptosoft).

678

679 **Fly Strains and Husbandry.** Wild-type and transgenic strains were maintained on standard yeast-  
680 agar-cornmeal medium at 25 °C. The following fly strains were used: *OregonR* and *PTEN*<sup>C076</sup>  
681 (Bloomington Stock Center, Indiana University), *UAS-dTrpA1* (Hamada et al., 2008), *UAS-SOD2*  
682 (Missirlis et al., 2003), *UAS-Catalase* (Missirlis et al., 2001), *UAS-Duox* (Ha, 2005), *DJ-11β*<sup>Δ93</sup>  
683 (Meulener et al., 2005), *UAS-DJ-1β*<sup>C104A</sup> (Meulener et al., 2006), UAS-RNAi lines targeting *SOD1*,  
684 *SOD2*, *Catalase* and *PTEN* (KK collection, Vienna Drosophila Resource Centre ) (Dietzl et al., 2007),  
685 *UAS-PI3K*<sup>DN</sup> (Leevers et al., 1996), *UAS-PTEN* (Gao et al., 2000). The following two GAL4 expression  
686 lines were used to target GAL4 to the aCC and RP2 motoneurons: *aCC-FLP-GAL4* (*everN2-Flippase*,  
687 *UAS-myr::mRFP1*, *UAS-Flp*, *tubulin84B-FRT-CD2-FRT-GAL4*) (Roy et al., 2007) expresses GAL4  
688 stochastically in single aCC and RP2 motoneurons allowing the imaging of aCC neurons in isolation,  
689 as required for dendritic arbor resolution and reconstruction. *aCC/RP2-GAL4* (*everN2-GAL4* (Fujioka  
690 et al., 2003), *UAS-myr-mRFP1*, *UAS-Flp*, *tubulin84B-FRT-CD2-FRT-GAL4*; *RRαGAL4*, *20xUAS-*  
691 *6XmCherry::HA* (Shearin et al., 2014)) was used for NMJ analysis as it expresses GAL4 in every aCC  
692 and RP2 motoneuron. *everN2-GAL4* expression is restricted to the embryo and FLPase-gated  
693 *tubulin84B-FRT-CD2-FRT-GAL4* maintains GAL4 expression at high levels during larval stages.

694

### 695 **Dissection and Immunocytochemistry**

696 **1<sup>st</sup> Instar Ventral Nerve Cord (VNC).** Flies were allowed to lay eggs on apple juice-based agar  
697 medium for 24 hrs at 25°C. Embryos were dechorionated using bleach (3.5 minutes room  
698 temperature) then incubated (25°C) in pre-warmed Sorensen's saline (pH 7.2, 0.075 M) whilst  
699 adhered to a petri dish. Hatched larvae (floating) were recovered hourly and transferred to pre-  
700 warmed apple-juice agar plates supplemented with yeast paste. Larvae were allowed to develop for  
701 a further 24 hrs (24 hrs after larval hatching, ALH) at 25°C, 27°C or 29°C prior to dissection in  
702 Sorensen's saline. A fine hypodermic needle (30 1/2 G; Microlance) was used as a scalpel to cut off  
703 the anterior end of each larva, allowing gut, fat body, and trachea to be removed. The ventral nerve  
704 chord and brain lobes, extruded with viscera upon decapitation, were dissected out and transferred  
705 to a cover glass coated with poly-L-lysine (Sigma-Aldrich), positioned dorsal side up in Sorensen's  
706 saline. A clean cover glass was placed on top of the preparation, with strips of double-sided sticky  
707 tape as spacers positioned along the edges.

708

709 **Wandering 3<sup>rd</sup> Instar.** Flies were allowed to lay eggs on apple-juice agar based medium overnight at  
710 25°C, larvae were then incubated at 25°C or 27°C until the late wandering 3<sup>rd</sup> instar stage. Larvae  
711 were reared on yeast paste colored with Bromophenol Blue Sodium Salt (Sigma-Aldrich) to allow  
712 visualization of gut-clearance, an indicator of the late wandering 3<sup>rd</sup> instar stage. For Di-ethylmaleate  
713 (DEM) (Sigma-Aldrich) and paraquat (Sigma-Aldrich) feeding, yeast paste was made using a 5 mM –  
714 15 mM aqueous solution. Larvae were ‘fillet’ dissected in Sorensen’s saline and fixed for 15 minutes  
715 at room temperature in 4% formaldehyde (in Sorensen’s saline). Specimens were then washed and  
716 stained in Sorensen’s saline containing 0.3% Triton X-100 (Sigma-Aldrich) using the following primary  
717 / secondary antibodies; Goat-anti-HRP Alexa Fluor 594 (1:400) (Jackson ImmunoResearch Cat. No.  
718 123-585-021), Rabbit-anti-dsRED (1:1200) (ClonTech Cat. No. 632496), Donkey-anti-Rabbit CF568  
719 (1:1200) (Biotium Cat. No. 20098) incubated overnight at 4°C or 2 hrs at room temperature.  
720 Specimens were mounted in EverBrite mounting medium (Biotium).

721

## 722 **Image Acquisition and Analysis**

723 **1<sup>st</sup> Instar Ventral Nerve Cord (VNC).** Ventral nerve cords were pre-screened for fluorescently  
724 labeled, isolated, aCC motoneurons using a Zeiss Axiophot compound epifluorescence microscope  
725 and a Zeiss Plan-Neofluar 40x/0.75 N.A. objective lens. Suitable VNCs were imaged immediately with  
726 a Yokagawa CSU-22 spinning disk confocal field scanner mounted on an Olympus BX51WI  
727 microscope, using a 60x/1.2 N.A. Olympus water immersion objective. Images were acquired with a  
728 voxel size of 0.2 × 0.2 × 0.3 μm using a QuantEM cooled EMCCD camera (Photometrics), operated via  
729 MetaMorph software (Molecular Devices). Dendritic trees were digitally reconstructed using Amira  
730 Resolve RT 4.1 (Visualization Sciences Group and Zuse Institute), supplemented with a 3D  
731 reconstruction algorithm (Evers et al., 2005; Schmitt et al., 2004), and images were processed using  
732 Amira and ImageJ (National Institutes of Health).

733

734 **Wandering 3<sup>rd</sup> Instar.** Dissected specimens were imaged using a Leica SP5 point-scanning confocal,  
735 and a 63x/1.3 N.A. (Leica) glycerol immersion objective lens and LAS AF (Leica Application Suite  
736 Advanced Fluorescence) software. Confocal images were processed using ImageJ and Photoshop  
737 (Adobe). Bouton number of the NMJ on muscle DA1 [1] from segments A3-A5 was determined by  
738 counting every distinct spherical varicosity along the NMJ branch. DA1 muscles were imaged using a  
739 Zeiss Axiophot compound microscope and a Zeiss Plan-Neofluar 10x/0.3 N.A. objective lens. Muscle  
740 surface area (MSA) was determined by multiplying muscle length by width using ImageJ. In order to  
741 correct for subtle differences in animal size (typically 5-10%) bouton number normalization was  
742 performed using the following calculation: (mean control MSA / mean experimental MSA) x test  
743 bouton number = normalized experimental bouton number.

744

745 **Ratiometric ROS Reporter.** *aCC/RP2-Gal4* was used to drive the expression of *UAS-mito-roGFP2-*  
746 *Orp1* (Albrecht et al., 2011; Gutscher et al., 2009) in all aCC and RP2 motoneurons. Wandering third  
747 instar larvae were fillet dissected in PBS-NEM (137mM NaCl, 2.7mM KCl, 10mM Na<sub>2</sub>HPO<sub>4</sub>, 1.8mM  
748 KH<sub>2</sub>PO<sub>4</sub>, 20mM N-ethylmaleimide (NEM), pH 7.4). Larval fillet preparations were incubated for 5  
749 minutes in PBS-NEM then fixed for 8 minutes in 4% formaldehyde (in PBS-NEM). Specimens were  
750 washed three times in PBS-NEM and then equilibrated in 70% glycerol. Specimens were mounted in  
751 glycerol and imaged the same day. Imaging was performed on a Leica SP5 point-scanning confocal,

752 using a 63x/1.3 N.A. (Leica) glycerol immersion objective lens. The reporter was excited sequentially  
753 at 405nm and 488nm (Albrecht et al., 2011) with emission detected at 500–535nm. 16-bit images  
754 were acquired using Leica LAS AF software and processed using ImageJ. Z-stack images were  
755 maximally projected and converted to 32-bit. To remove fringing artefacts around bouton edges  
756 488nm images were thresholded using the ‘Intermodes’ algorithm with values below threshold set  
757 to ‘not a number’, and ratio images were created by dividing the 405nm image by the 488nm image  
758 pixel by pixel (Albrecht et al., 2011). Regions of Interest were taken on the ratio image spanning the  
759 entire NMJ and the mean value obtained from each NMJ was used for statistical analysis.

760

761 **Transmission Electron Microscopy.** Third instar wandering larvae were fillet dissected in PBS and  
762 fixed overnight in 0.1M NaPO<sub>4</sub>, pH 7.4, 1% glutaraldehyde, and 4% formaldehyde, pH 7.3. Fixed  
763 specimens were washed 3× in 0.1M NaPO<sub>4</sub> before incubation in OsO<sub>4</sub> (1% in 0.1M NaPO<sub>4</sub>; 2hr).  
764 Preparations were washed 3× in distilled water, incubated in 1% uranyl acetate, then washed again  
765 (3× distilled water) and dehydrated through a graded ethanol series: 20% increments starting at  
766 30% followed by two 100% changes and then 2× 100% propylene oxide. Specimens were incubated  
767 in a graded series of epon araldite resin (in propylene oxide): 25% increments culminating in 3×  
768 100% changes. Individual muscles were then dissected and transferred into embedding molds,  
769 followed by polymerization at 60°C for 48 hrs. Resin mounted specimens were sectioned (60–70  
770 nm) using glass knives upon a microtome (Ultracut UCT; Leica). Sections were placed onto grids,  
771 incubated in uranyl acetate (50% in ethanol), washed in distilled water and incubated in lead  
772 citrate. Sections were imaged using a transmission electron microscope (TECNAI 12 G<sup>2</sup>; FEI) with a  
773 camera (Soft Imaging Solutions MegaView; Olympus) and Tecnai user interface v2.1.8 and analySIS  
774 v3.2 (Soft Imaging Systems).

775

#### 776 **Behavior – larval crawling analysis**

777 To record larval crawling, mid-3<sup>rd</sup> instar larvae (72hrs ALH) were briefly rinsed in water to remove  
778 any food and yeast residues, then up to 12 larvae were placed into a 24cm x 24cm arena of 0.8%  
779 agar in water, poured to 5 mm thickness. Crawling behavior was recorded in a temperature and  
780 humidity controlled incubator at temperatures ranging from 25-32°C, as indicated for each  
781 experiment. Larvae were allowed to acclimatise for 5 minutes, then recorded for 15 minutes under  
782 infrared LED illumination (intensity from 14.33 nW/mm<sup>2</sup> in the edge to 9.12 nW/mm<sup>2</sup> in the center),  
783 using frustrated total internal reflection using a modified FIM tracker (36) [https://www.uni-](https://www.uni-muenster.de/PRIA/en/FIM/index.html)  
784 [muenster.de/PRIA/en/FIM/index.html](https://www.uni-muenster.de/PRIA/en/FIM/index.html). Larvae were recorded with a Basler acA2040-180km CMOS  
785 camera using Pylon and StreamPix software, mounted with a 16mm KOWA IJM3sHC.SW VIS-NIR  
786 Lens. Images were acquired at 5 frames per second. For each larvae, average crawling speed was  
787 calculated from long, uninterrupted forward crawls identified manually using FIMTrack. The 15  
788 minute recording period was partitioned into 5 minute sections with each larvae being assayed once  
789 within each section, allowing each specimen to be sampled a maximum of 3 times. We observed no  
790 change in average crawling speed within the duration of the 15-minute recording.

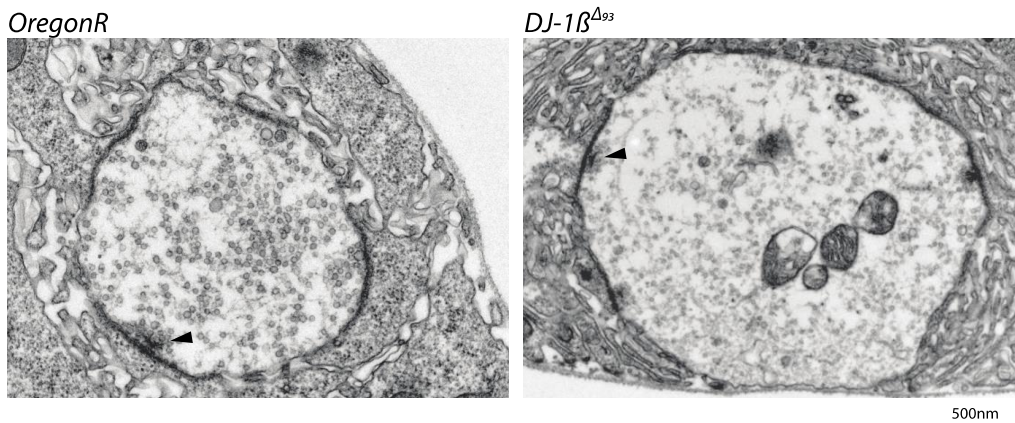
791

792 **Data Analysis.** All data handling was performed using Prism software (GraphPad). NMJ bouton  
793 number and ratiometric ROS reporter data were tested for normal / Gaussian distribution using the  
794 D’Agostino-Pearson omnibus normality test. Due to a lower replicate number, dendritic arbor

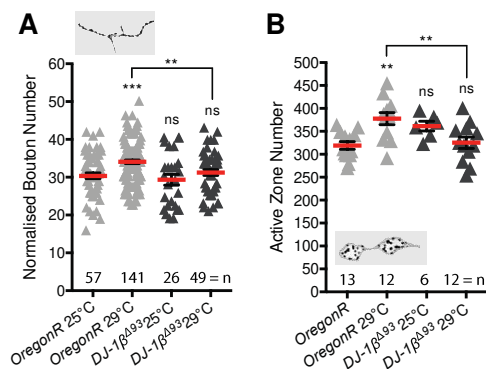
795 reconstruction data were tested for normality using the Kolmogorov-Smirnov with Dallal-Wilkinson-  
 796 Lilliefors P value test. Normal distribution was thus confirmed for all data presented, which were  
 797 compared using one-way analysis of variance (ANOVA), with Tukey's multiple comparisons test  
 798 where \*P<0.05, \*\*P<0.01, \*\*\*P<0.001, \*\*\*\*P<0.0001.

799  
 800  
 801  
 802  
 803  
 804  
 805

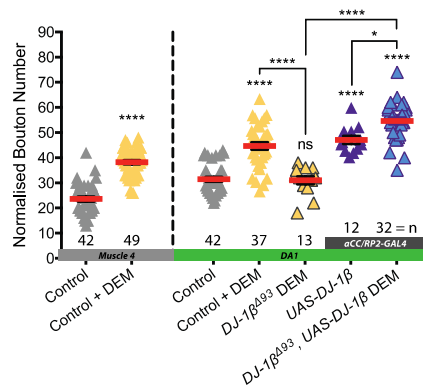
**Supplementary Figures**



806  
 807 **Figure 3-Figure Supplement 1:** *DJ-1β<sup>Δ93</sup>* mutant 3<sup>rd</sup> instar larval NMJs are phenotypically normal.  
 808 Representative TEM bouton cross-sectional images showing that pre-synaptic architecture is intact  
 809 including active-zones with associated clustered synaptic vesicles (arrowed).  
 810



811  
 812  
 813 **Figure 3-Figure Supplement 2: A.** *DJ-1β* null mutant (*DJ-1β<sup>Δ93</sup>*) larvae do not show systemic activity-  
 814 dependent NMJ elaboration. Normalised bouton number dot plot showing significantly increased  
 815 NMJ elaboration in *OregonR*, but not *DJ-1β<sup>Δ93</sup>*, larvae reared at 29°C vs 25°C. **B.** *DJ-1β<sup>Δ93</sup>* larvae also  
 816 do not show systemic activity-dependent increase in active zone number. *OregonR*, but not *DJ-1β<sup>Δ93</sup>*,  
 817 show significantly increased NMJ active zone number when reared at 29°C vs 25°C. Mean +/- SEM,  
 818 ANOVA \*\*p<0.01, \*\*\*p<0.001, n=replicate number.  
 819



820

821

822 **Figure 3-Figure Supplement 3:** 10mM DEM feeding induces increased bouton number at both  
 823 muscle 4 and DA1. This response is absent in *DJ-1β* null mutant larvae and is re-established via  
 824 neuronal (*aCC* and *RP2*) specific miss-expression of *UAS-DJ-1β*. *UAS-DJ-1β* expression alone elevates  
 825 bouton number, which is exacerbated when combined with DEM feeding. Normalised bouton  
 826 number dot plot, Control is *aCC-FLP-GAL4* alone in heterozygous condition. Mean +/- SEM, ANOVA  
 827 \*p<0.05, \*\*\*\*p<0.0001, n=replicate number.

828

829

830 **References**

831

832 **Adler, V., Yin, Z., Fuchs, S. Y., Benezra, M., Rosario, L., Tew, K. D., Pincus, M. R., Sardana, M.,**  
833 **Henderson, C. J., Wolf, C. R., et al.** (1999). Regulation of JNK signaling by GSTp. *EMBO J* **18**,  
834 1321–1334.

835 **Albrecht, S. C., Barata, A. G., Grosshans, J., Teleman, A. A. and Dick, T. P.** (2011). In vivo mapping  
836 of hydrogen peroxide and oxidized glutathione reveals chemical and regional specificity of redox  
837 homeostasis. *Cell Metab* **14**, 819–829.

838 **Ariga, H., Takahashi-Niki, K., Kato, I., Maita, H., Niki, T. and Iguchi-Ariga, S. M. M.** (2013).  
839 Neuroprotective function of DJ-1 in Parkinson's disease. *Oxid Med Cell Longev* **2013**, 683920.

840 **Ataman, B., Ashley, J., Gorczyca, M., Ramachandran, P., Fouquet, W., Sigrist, S. J. and Budnik, V.**  
841 (2008). Rapid activity-dependent modifications in synaptic structure and function require  
842 bidirectional Wnt signaling. *Neuron* **57**, 705–718.

843 **Attwell, D. and Laughlin, S. B.** (2001). An energy budget for signaling in the grey matter of the  
844 brain. *J. Cereb. Blood Flow Metab.* **21**, 1133–1145.

845 **Baines, R. A., Robinson, S. G., Fujioka, M., Jaynes, J. B. and Bate, M.** (1999). Postsynaptic  
846 expression of tetanus toxin light chain blocks synaptogenesis in *Drosophila*. *Curr Biol* **9**, 1267–  
847 1270.

848 **Baines, R. A., Uhler, J. P., Thompson, A., Sweeney, S. T. and Bate, M.** (2001). Altered electrical  
849 properties in *Drosophila* neurons developing without synaptic transmission. *J Neurosci* **21**,  
850 1523–1531.

851 **Bate, M.** (1993). The mesoderm and its derivatives. In *The Development of Drosophila melanogaster*.  
852 (eds. Bate, C. M. and Martinez-Arias, A., Cold Spring Harbor: The development of *Drosophila*  
853 *melanogaster*.

854 **Bayat, V., Jaiswal, M. and Bellen, H. J.** (2011). The BMP signaling pathway at the *Drosophila*  
855 neuromuscular junction and its links to neurodegenerative diseases. *Curr Opin Neurobiol* **21**,  
856 182–188.

857 **Bánfi, B., Tirone, F., Durussel, I., Knisz, J., Moskwa, P., Molnár, G. Z., Krause, K.-H. and Cox, J. A.**  
858 (2004). Mechanism of Ca<sup>2+</sup> activation of the NADPH oxidase 5 (NOX5). *J Biol Chem* **279**, 18583–  
859 18591.

860 **Bell, K. F. S., Al-Mubarak, B., Martel, M.-A., McKay, S., Wheelan, N., Hasel, P., Márkus, N. M.,**  
861 **Baxter, P., Deighton, R. F., Serio, A., et al.** (2015). Neuronal development is promoted by  
862 weakened intrinsic antioxidant defences due to epigenetic repression of Nrf2. *Nat Comms* **6**,  
863 7066.

864 **Berke, B., Wittnam, J., McNeill, E., Van Vactor, D. L. and Keshishian, H.** (2013). Retrograde BMP  
865 signaling at the synapse: a permissive signal for synapse maturation and activity-dependent  
866 plasticity. *J Neurosci* **33**, 17937–17950.

867 **Bindokas, V. P., Jordán, J., Lee, C. C. and Miller, R. J.** (1996). Superoxide production in rat  
868 hippocampal neurons: selective imaging with hydroethidine. *J. Neurosci.* **16**, 1324–1336.

869 **Blackinton, J., Lakshminarasimhan, M., Thomas, K. J., Ahmad, R., Greggio, E., Raza, A. S.,**  
870 **Cookson, M. R. and Wilson, M. A.** (2009). Formation of a stabilized cysteine sulfinic acid is  
871 critical for the mitochondrial function of the parkinsonism protein DJ-1. *J Biol Chem* **284**, 6476–  
872 6485.

873 **Bonifati, V., Rizzu, P., van Baren, M. J., Schaap, O., Breedveld, G. J., Krieger, E., Dekker, M. C. J.,**  
874 **Squitieri, F., Ibanez, P., Joesse, M., et al.** (2003). Mutations in the DJ-1 gene associated with  
875 autosomal recessive early-onset parkinsonism. *Science* **299**, 256–259.

876 **Brennan, A. M., Won Suh, S., Joon Won, S., Narasimhan, P., Kauppinen, T. M., Lee, H., Edling, Y.,**  
877 **Chan, P. H. and Swanson, R. A.** (2009). NADPH oxidase is the primary source of superoxide  
878 induced by NMDA receptor activation. *Nat Neurosci* **12**, 857–863.

879 **Brierley, D. J., Blanc, E., Reddy, O. V., VijayRaghavan, K. and Williams, D. W.** (2009). Dendritic  
880 targeting in the leg neuropil of *Drosophila*: the role of midline signalling molecules in generating  
881 a myotopic map. *PLoS Biol* **7**, e1000199.

882 **Budnik, V. and Salinas, P. C.** (2011). Wnt signaling during synaptic development and plasticity. *Curr*  
883 *Opin Neurobiol* **21**, 151–159.

884 **Cali, T., Ottolini, D., Soriano, M. E. and Brini, M.** (2015). A new split-GFP-based probe reveals DJ-1  
885 translocation into the mitochondrial matrix to sustain ATP synthesis upon nutrient deprivation.  
886 *Hum Mol Genet* **24**, 1045–1060.

887 **Campbell, M. and Ganetzky, B.** (2012). Extensive morphological divergence and rapid evolution of  
888 the larval neuromuscular junction in *Drosophila*. *Proc Natl Acad Sci U S A*.

889 **Canet-Avilés, R. M. and Wilson, M. A.** (2004). The Parkinson's disease protein DJ-1 is  
890 neuroprotective due to cysteine-sulfinic acid-driven mitochondrial localization.

891 **Chandrasekaran, V., Lea, C., Sosa, J. C., Higgins, D. and Lein, P. J.** (2015). Reactive oxygen species  
892 are involved in BMP-induced dendritic growth in cultured rat sympathetic neurons. *Mol Cell*  
893 *Neurosci* **67**, 116–125.

894 **Cho, R. W., Buhl, L. K., Volfson, D., Tran, A., Li, F., Akbergenova, Y. and Littleton, J. T.** (2015).  
895 Phosphorylation of Complexin by PKA Regulates Activity-Dependent Spontaneous  
896 Neurotransmitter Release and Structural Synaptic Plasticity. *Neuron* **88**, 749–761.

897 **Choi, J. C., Park, D. and Griffith, L. C.** (2004). Electrophysiological and morphological  
898 characterization of identified motor neurons in the *Drosophila* third instar larva central nervous  
899 system. *J Neurophysiol* **91**, 2353–2365.

900 **Chouhan, A. K., Zhang, J., Zinsmaier, K. E. and Macleod, G. T.** (2010). Presynaptic mitochondria in  
901 functionally different motor neurons exhibit similar affinities for Ca<sup>2+</sup> but exert little influence  
902 as Ca<sup>2+</sup> buffers at nerve firing rates in situ. *J Neurosci* **30**, 1869–1881.

903 **Crossley, A. C.** (1978). Morphology and development of the *Drosophila* muscular system. In *Genetics*  
904 *and biology of Drosophila* (eds. Ashburner, M. and Wright, T., pp. 499–560. New York: Genetics  
905 and biology of *Drosophila*.

906 **Davis, G. W.** (2006). Homeostatic control of neural activity: from phenomenology to molecular  
907 design. *Annu Rev Neurosci* **29**, 307–323.

- 908 **Davis, G. W. and Müller, M.** (2015). Homeostatic control of presynaptic neurotransmitter release.  
909 *Annu Rev Physiol* **77**, 251–270.
- 910 **Davis, G. W., DiAntonio, A., Petersen, S. A. and Goodman, C. S.** (1998). Postsynaptic PKA controls  
911 quantal size and reveals a retrograde signal that regulates presynaptic transmitter release in  
912 *Drosophila*. *Neuron* **20**, 305–315.
- 913 **Davis, G. W., Schuster, C. M. and Goodman, C. S.** (1996). Genetic dissection of structural and  
914 functional components of synaptic plasticity. III. CREB is necessary for presynaptic functional  
915 plasticity. *Neuron* **17**, 669–679.
- 916 **Davydova, D., Marini, C., King, C., Klueva, J., Bischof, F., Romorini, S., Montenegro-Venegas, C.,**  
917 **Heine, M., Schneider, R., Schröder, M. S., et al.** (2014). Bassoon specifically controls presynaptic  
918 P/Q-type Ca<sup>2+</sup> channels via RIM-binding protein. *Neuron* **82**, 181–194.
- 919 **Dietzl, G., Chen, D., Schnorrer, F., Su, K.-C., Barinova, Y., Fellner, M., Gasser, B., Kinsey, K.,**  
920 **Oppel, S., Scheiblaue, S., et al.** (2007). A genome-wide transgenic RNAi library for conditional  
921 gene inactivation in *Drosophila*. *Nature* **448**, 151–156.
- 922 **Dillon, M. E., Wang, G., Garrity, P. A. and Huey, R. B.** (2009). Review: Thermal preference in  
923 *Drosophila*. *J. Therm. Biol.* **34**, 109–119.
- 924 **Do, K. Q., Cuenod, M. and Hensch, T. K.** (2015). Targeting Oxidative Stress and Aberrant Critical  
925 Period Plasticity in the Developmental Trajectory to Schizophrenia. *Schizophr Bull* **41**, 835–846.
- 926 **Driscoll, H. E., Muraro, N. I., He, M. and Baines, R. A.** (2013). Pumilio-2 regulates translation of  
927 nav1.6 to mediate homeostasis of membrane excitability. *J Neurosci* **33**, 9644–9654.
- 928 **Dugan, L. L., Sensi, S. L., Canzoniero, L. M., Handran, S. D., Rothman, S. M., Lin, T. S., Goldberg,**  
929 **M. P. and Choi, D. W.** (1995). Mitochondrial production of reactive oxygen species in cortical  
930 neurons following exposure to N-methyl-D-aspartate. *J. Neurosci.* **15**, 6377–6388.
- 931 **Evers, J. F., Schmitt, S., Sibila, M. and Duch, C.** (2005). Progress in functional neuroanatomy:  
932 precise automatic geometric reconstruction of neuronal morphology from confocal image  
933 stacks. *J Neurophysiol* **93**, 2331–2342.
- 934 **Finkel, T.** (2011). Signal transduction by reactive oxygen species. *J Cell Biol* **194**, 7–15.
- 935 **Finkel, T. and Holbrook, N. J.** (2000). Oxidants, oxidative stress and the biology of ageing. *Nature*  
936 **408**, 239–247.
- 937 **Frank, C. A.** (2014). Homeostatic plasticity at the *Drosophila* neuromuscular junction.  
938 *Neuropharmacology* **78**, 63–74.
- 939 **Frank, C. A., Kennedy, M. J., Goold, C. P., Marek, K. W. and Davis, G. W.** (2006). Mechanisms  
940 underlying the rapid induction and sustained expression of synaptic homeostasis. *Neuron* **52**,  
941 663–677.
- 942 **Frank, C. A., Pielage, J. and Davis, G. W.** (2009). A presynaptic homeostatic signaling system  
943 composed of the Eph receptor, ephexin, Cdc42, and CaV2.1 calcium channels. *Neuron* **61**, 556–  
944 569.

- 945 **Frank, C. A., Wang, X., Collins, C. A., Rodal, A. A., Yuan, Q., Verstreken, P. and Dickman, D. K.**  
946 (2013). New approaches for studying synaptic development, function, and plasticity using  
947 *Drosophila* as a model system. *J Neurosci* **33**, 17560–17568.
- 948 **Fujioka, M., Lear, B. C., Landgraf, M., Yusibova, G. L., Zhou, J., Riley, K. M., Patel, N. H. and**  
949 **Jaynes, J. B.** (2003). Even-skipped, acting as a repressor, regulates axonal projections in  
950 *Drosophila*. *Development* **130**, 5385–5400.
- 951 **Funato, Y., Michiue, T., Asashima, M. and Miki, H.** (2006). The thioredoxin-related redox-regulating  
952 protein nucleoredoxin inhibits Wnt-beta-catenin signalling through dishevelled. *Nat Cell Biol* **8**,  
953 501–508.
- 954 **Fushiki, A., Zwart, M. F., Kohsaka, H., Fetter, R. D., Cardona, A. and Nose, A.** (2016). A circuit  
955 mechanism for the propagation of waves of muscle contraction in *Drosophila*. *Elife* **5**.
- 956 **Gahtan, E., Auerbach, J. M., Groner, Y. and Segal, M.** (1998). Reversible impairment of long-term  
957 potentiation in transgenic Cu/Zn-SOD mice. *Eur J Neurosci* **10**, 538–544.
- 958 **Gao, X., Neufeld, T. P. and Pan, D.** (2000). *Drosophila* PTEN regulates cell growth and proliferation  
959 through PI3K-dependent and -independent pathways. *Dev Biol* **221**, 404–418.
- 960 **Gaviño, M. A., Ford, K. J., Archila, S. and Davis, G. W.** (2015). Homeostatic synaptic depression is  
961 achieved through a regulated decrease in presynaptic calcium channel abundance. *Elife* **4**.
- 962 **Giachello, C. N. and Baines, R. A.** (2016). Regulation of motoneuron excitability and the setting of  
963 homeostatic limits. *Curr Opin Neurobiol* **43**, 1–6.
- 964 **Giniatullin, A. R., Darios, F., Shakirzyanova, A., Davletov, B. and Giniatullin, R.** (2006). SNAP25 is  
965 a pre-synaptic target for the depressant action of reactive oxygen species on transmitter  
966 release. *J Neurochem* **98**, 1789–1797.
- 967 **Gladyshev, V. N.** (2014). The free radical theory of aging is dead. Long live the damage theory!  
968 *Antioxid Redox Signal* **20**, 727–731.
- 969 **Gutscher, M., Sobotta, M. C., Wabnitz, G. H., Ballikaya, S., Meyer, A. J., Samstag, Y. and Dick, T. P.**  
970 (2009). Proximity-based protein thiol oxidation by H<sub>2</sub>O<sub>2</sub>-scavenging peroxidases. *J Biol Chem*  
971 **284**, 31532–31540.
- 972 **Ha, E. M.** (2005). A Direct Role for Dual Oxidase in *Drosophila* Gut Immunity. *Science* **310**, 847–850.
- 973 **Hallermann, S., de Kock, C. P. J., Stuart, G. J. and Kole, M. H. P.** (2012). State and location  
974 dependence of action potential metabolic cost in cortical pyramidal neurons. *Nat Neurosci* **15**,  
975 1007–1014.
- 976 **Halliwell, B.** (1992). Reactive oxygen species and the central nervous system. *J Neurochem* **59**, 1609–  
977 1623.
- 978 **Hamada, F. N., Rosenzweig, M., Kang, K., Pulver, S. R., Ghezzi, A., Jegla, T. J. and Garrity, P. A.**  
979 (2008). An internal thermal sensor controlling temperature preference in *Drosophila*. *Nature*  
980 **454**, 217–220.
- 981 **Hao, L.-Y., Giasson, B. I. and Bonini, N. M.** (2010). DJ-1 is critical for mitochondrial function and  
982 rescues PINK1 loss of function. *Proc Natl Acad Sci U S A* **107**, 9747–9752.

- 983 **HARMAN, D.** (1956). Aging: a theory based on free radical and radiation chemistry. *J Gerontol* **11**,  
984 298–300.
- 985 **Harris, K. P. and Littleton, J. T.** (2015). Transmission, Development, and Plasticity of Synapses.  
986 *Genetics* **201**, 345–375.
- 987 **Hartwig, C. L., Worrell, J., Levine, R. B., Ramaswami, M. and Sanyal, S.** (2008). Normal dendrite  
988 growth in Drosophila motor neurons requires the AP-1 transcription factor. *Dev Neurobiol* **68**,  
989 1225–1242.
- 990 **Hoang, B. and Chiba, A.** (2001). Single-cell analysis of Drosophila larval neuromuscular synapses.  
991 *Dev Biol* **229**, 55–70.
- 992 **Hongpaisan, J., Winters, C. A. and Andrews, S. B.** (2004). Strong calcium entry activates  
993 mitochondrial superoxide generation, upregulating kinase signaling in hippocampal neurons. *J*  
994 *Neurosci* **24**, 10878–10887.
- 995 **Höhn, A. and Grune, T.** (2013). Lipofuscin: formation, effects and role of macroautophagy. *Redox*  
996 *Biol* **1**, 140–144.
- 997 **Huddleston, A. T., Tang, W., Takeshima, H., Hamilton, S. L. and Klann, E.** (2008). Superoxide-  
998 induced potentiation in the hippocampus requires activation of ryanodine receptor type 3 and  
999 ERK. *J Neurophysiol* **99**, 1565–1571.
- 1000 **Itakura, Y., Kohsaka, H., Ohyama, T., Zlatic, M., Pulver, S. R. and Nose, A.** (2015). Identification of  
1001 Inhibitory Premotor Interneurons Activated at a Late Phase in a Motor Cycle during Drosophila  
1002 Larval Locomotion. *PLoS ONE* **10**, e0136660.
- 1003 **Jindra, M., Gaziouva, I., Uhlirova, M., Okabe, M., Hiromi, Y. and Hirose, S.** (2004). Coactivator  
1004 MBF1 preserves the redox-dependent AP-1 activity during oxidative stress in Drosophila. *EMBO*  
1005 *J* **23**, 3538–3547.
- 1006 **Jordán-Álvarez, S., Fouquet, W., Sigrist, S. J. and Acebes, A.** (2012). Presynaptic PI3K activity  
1007 triggers the formation of glutamate receptors at neuromuscular terminals of Drosophila. *J Cell*  
1008 *Sci* **125**, 3621–3629.
- 1009 **Kamsler, A. and Segal, M.** (2003a). Hydrogen peroxide modulation of synaptic plasticity. *J Neurosci*  
1010 **23**, 269–276.
- 1011 **Kamsler, A. and Segal, M.** (2003b). Paradoxical actions of hydrogen peroxide on long-term  
1012 potentiation in transgenic superoxide dismutase-1 mice. *J Neurosci* **23**, 10359–10367.
- 1013 **Kim, R. H., Peters, M., Jang, Y., Shi, W., Pintilie, M., Fletcher, G. C., DeLuca, C., Liepa, J., Zhou, L.,**  
1014 **Snow, B., et al.** (2005). DJ-1, a novel regulator of the tumor suppressor PTEN. *Cancer Cell* **7**,  
1015 263–273.
- 1016 **Kim, S. M., Kumar, V., Lin, Y. Q., Karunanithi, S. and Ramaswami, M.** (2009a). Fos and Jun  
1017 potentiate individual release sites and mobilize the reserve synaptic vesicle pool at the  
1018 Drosophila larval motor synapse. *Proc Natl Acad Sci U S A* **106**, 4000–4005.
- 1019 **Kim, Y.-C., Kitaura, H., Taira, T., Iguchi-Arigo, S. M. M. and Ariga, H.** (2009b). Oxidation of DJ-1-  
1020 dependent cell transformation through direct binding of DJ-1 to PTEN. *Int J Oncol* **35**, 1331–  
1021 1341.

- 1022 **Kishida, K. T., Hoeffler, C. A., Hu, D., Pao, M., Holland, S. M. and Klann, E.** (2006). Synaptic  
1023 plasticity deficits and mild memory impairments in mouse models of chronic granulomatous  
1024 disease. *Mol Cell Biol* **26**, 5908–5920.
- 1025 **Klann, E.** (1998). Cell-permeable scavengers of superoxide prevent long-term potentiation in  
1026 hippocampal area CA1. *J Neurophysiol* **80**, 452–457.
- 1027 **Knapp, L. T. and Klann, E.** (2002). Potentiation of hippocampal synaptic transmission by superoxide  
1028 requires the oxidative activation of protein kinase C. *J Neurosci* **22**, 674–683.
- 1029 **Kohsaka, H., Okusawa, S., Itakura, Y., Fushiki, A. and Nose, A.** (2012). Development of larval  
1030 motor circuits in *Drosophila*. *Dev Growth Differ* **54**, 408–419.
- 1031 **Kohsaka, H., Takasu, E., Morimoto, T. and Nose, A.** (2014). A group of segmental premotor  
1032 interneurons regulates the speed of axial locomotion in *Drosophila* larvae. *Curr Biol* **24**, 2632–  
1033 2642.
- 1034 **Koles, K. and Budnik, V.** (2012). Wnt signaling in neuromuscular junction development. *Cold Spring*  
1035 *Harb Perspect Biol* **4**.
- 1036 **Landgraf, M., Jeffrey, V., Fujioka, M., Jaynes, J. B. and Bate, M.** (2003). Embryonic origins of a  
1037 motor system: motor dendrites form a myotopic map in *Drosophila*. *PLoS Biol* **1**, E41.
- 1038 **Lazarevic, V., Schöne, C., Heine, M., Gundelfinger, E. D. and Fejtova, A.** (2011). Extensive  
1039 remodeling of the presynaptic cytomatrix upon homeostatic adaptation to network activity  
1040 silencing. *J Neurosci* **31**, 10189–10200.
- 1041 **Lee, K. Y., Chung, K. and Chung, J. M.** (2010). Involvement of reactive oxygen species in long-term  
1042 potentiation in the spinal cord dorsal horn. *J Neurophysiol* **103**, 382–391.
- 1043 **Leevers, S. J., Weinkove, D., MacDougall, L. K., Hafen, E. and Waterfield, M. D.** (1996). The  
1044 *Drosophila* phosphoinositide 3-kinase Dp110 promotes cell growth. *EMBO J* **15**, 6584–6594.
- 1045 **Levin, E. D., Brady, T. C., Hochrein, E. C., Oury, T. D., Jonsson, L. M., Marklund, S. L. and Crapo, J.**  
1046 **D.** (1998). Molecular manipulations of extracellular superoxide dismutase: functional  
1047 importance for learning. *Behav. Genet.* **28**, 381–390.
- 1048 **Liemburg-Apers, D. C., Willems, P. H. G. M., Koopman, W. J. H. and Grefte, S.** (2015). Interactions  
1049 between mitochondrial reactive oxygen species and cellular glucose metabolism. *Arch. Toxicol.*  
1050 **89**, 1209–1226.
- 1051 **Lin, J., Prahlad, J. and Wilson, M. A.** (2012a). Conservation of oxidative protein stabilization in an  
1052 insect homologue of parkinsonism-associated protein DJ-1. *Biochemistry* **51**, 3799–3807.
- 1053 **Lin, W.-H., Günay, C., Marley, R., Prinz, A. A. and Baines, R. A.** (2012b). Activity-dependent  
1054 alternative splicing increases persistent sodium current and promotes seizure. *J Neurosci* **32**,  
1055 7267–7277.
- 1056 **Loebrich, S. and Nedivi, E.** (2009). The function of activity-regulated genes in the nervous system.  
1057 *Physiol Rev* **89**, 1079–1103.

- 1058 **Love, N. R., Chen, Y., Ishibashi, S., Kritsiligkou, P., Lea, R., Koh, Y., Gallop, J. L., Dorey, K. and**  
1059 **Amaya, E.** (2013). Amputation-induced reactive oxygen species are required for successful  
1060 Xenopus tadpole tail regeneration. *Nat Cell Biol.*
- 1061 **Luo, J., Shen, W. L. and Montell, C.** (2016). TRPA1 mediates sensation of the rate of temperature  
1062 change in Drosophila larvae. *Nat Neurosci.*
- 1063 **Marrus, S. B. and DiAntonio, A.** (2005). Investigating the safety factor at an invertebrate  
1064 neuromuscular junction. *J Neurobiol* **63**, 62–69.
- 1065 **Martins, R. N., Harper, C. G., Stokes, G. B. and Masters, C. L.** (1986). Increased cerebral glucose-6-  
1066 phosphate dehydrogenase activity in Alzheimer's disease may reflect oxidative stress. *J*  
1067 *Neurochem* **46**, 1042–1045.
- 1068 **Martín-Peña, A., Acebes, A., Rodríguez, J.-R., Sorribes, A., de Polavieja, G. G., Fernández-Fúnez,**  
1069 **P. and Ferrús, A.** (2006). Age-independent synaptogenesis by phosphoinositide 3 kinase. *J*  
1070 *Neurosci* **26**, 10199–10208.
- 1071 **Massaad, C. A. and Klann, E.** (2011). Reactive oxygen species in the regulation of synaptic plasticity  
1072 and memory. *Antioxid Redox Signal* **14**, 2013–2054.
- 1073 **Matz, J., Gilyan, A., Kolar, A., McCarvill, T. and Krueger, S. R.** (2010). Rapid structural alterations  
1074 of the active zone lead to sustained changes in neurotransmitter release. *Proc Natl Acad Sci U S*  
1075 *A* **107**, 8836–8841.
- 1076 **Mauss, A., Tripodi, M., Evers, J. F. and Landgraf, M.** (2009). Midline signalling systems direct the  
1077 formation of a neural map by dendritic targeting in the Drosophila motor system. *PLoS Biol* **7**,  
1078 e1000200.
- 1079 **Mee, C. J., Pym, E. C. G., Moffat, K. G. and Baines, R. A.** (2004). Regulation of neuronal excitability  
1080 through pumilio-dependent control of a sodium channel gene. *J Neurosci* **24**, 8695–8703.
- 1081 **Meulener, M. C., Xu, K., Thomson, L., Thompson, L., Ischiropoulos, H. and Bonini, N. M.** (2006).  
1082 Mutational analysis of DJ-1 in Drosophila implicates functional inactivation by oxidative damage  
1083 and aging. *Proc Natl Acad Sci USA* **103**, 12517–12522.
- 1084 **Meulener, M., Whitworth, A. J., Armstrong-Gold, C. E., Rizzu, P., Heutink, P., Wes, P. D., Pallanck,**  
1085 **L. J. and Bonini, N. M.** (2005). Drosophila DJ-1 mutants are selectively sensitive to  
1086 environmental toxins associated with Parkinson's disease. *Curr Biol* **15**, 1572–1577.
- 1087 **Milton, V. J. and Sweeney, S. T.** (2012). Oxidative stress in synapse development and function. *Dev*  
1088 *Neurobiol* **72**, 100–110.
- 1089 **Milton, V. J., Jarrett, H. E., Gowers, K., Chalak, S., Briggs, L., Robinson, I. M. and Sweeney, S. T.**  
1090 (2011). Oxidative stress induces overgrowth of the Drosophila neuromuscular junction. *Proc Natl*  
1091 *Acad Sci U S A* **108**, 17521–17526.
- 1092 **Missirlis, F., Phillips, J. P. and Jäckle, H.** (2001). Cooperative action of antioxidant defense systems  
1093 in Drosophila. *Current Biology* **11**, 1272–1277.
- 1094 **Missirlis, F., Rahlfs, S., Dimopoulos, N., Bauer, H., Becker, K., Hilliker, A., Phillips, J. P. and Jäckle,**  
1095 **H.** (2003). A putative glutathione peroxidase of Drosophila encodes a thioredoxin peroxidase  
1096 that provides resistance against oxidative stress but fails to complement a lack of catalase  
1097 activity. *Biol Chem* **384**, 463–472.

- 1098 **Munnamalai, V. and Suter, D. M.** (2009). Reactive oxygen species regulate F-actin dynamics in  
1099 neuronal growth cones and neurite outgrowth. *J Neurochem* **108**, 644–661.
- 1100 **Munnamalai, V., Weaver, C. J., Weisheit, C. E., Venkatraman, P., Agim, Z. S., Quinn, M. T. and**  
1101 **Suter, D. M.** (2014). Bidirectional interactions between NOX2-type NADPH oxidase and the F-  
1102 actin cytoskeleton in neuronal growth cones. *J Neurochem* **130**, 526–540.
- 1103 **Müller, M. and Davis, G. W.** (2012). Transsynaptic control of presynaptic Ca<sup>2+</sup> influx achieves  
1104 homeostatic potentiation of neurotransmitter release. *Curr Biol* **22**, 1102–1108.
- 1105 **Nagakubo, D., Taira, T., Kitaura, H., Ikeda, M., Tamai, K., Iguchi-Ariga, S. M. and Ariga, H.** (1997).  
1106 DJ-1, a novel oncogene which transforms mouse NIH3T3 cells in cooperation with ras. *Biochem*  
1107 *Biophys Res Commun* **231**, 509–513.
- 1108 **O'Leary, T., Williams, A. H., Caplan, J. S. and Marder, E.** (2013). Correlations in ion channel  
1109 expression emerge from homeostatic tuning rules. *Proc Natl Acad Sci U S A* **110**, E2645–54.
- 1110 **Olguín-Albuerne, M. and Morán, J.** (2015). ROS produced by NOX2 control in vitro development of  
1111 cerebellar granule neurons development. *ASN Neuro* **7**.
- 1112 **Osses, N. and Henriquez, J. P.** (2014). Bone morphogenetic protein signaling in vertebrate motor  
1113 neurons and neuromuscular communication. *Front Cell Neurosci* **8**, 453.
- 1114 **Ou, Y., Chwalla, B., Landgraf, M. and van Meyel, D. J.** (2008). Identification of genes influencing  
1115 dendrite morphogenesis in developing peripheral sensory and central motor neurons. *Neural*  
1116 *development* **3**, 16.
- 1117 **Owald, D., Lin, S. and Waddell, S.** (2015). Light, heat, action: neural control of fruit fly behaviour.  
1118 *Philos Trans R Soc Lond, B, Biol Sci* **370**, 20140211.
- 1119 **Pandey, D., Gratton, J.-P., Rafikov, R., Black, S. M. and Fulton, D. J. R.** (2011). Calcium/calmodulin-  
1120 dependent kinase II mediates the phosphorylation and activation of NADPH oxidase 5. *Mol.*  
1121 *Pharmacol.* **80**, 407–415.
- 1122 **Peled, E. S., Newman, Z. L. and Isacoff, E. Y.** (2014). Evoked and spontaneous transmission favored  
1123 by distinct sets of synapses. *Curr Biol* **24**, 484–493.
- 1124 **Peng, T.-I. and Jou, M.-J.** (2010). Oxidative stress caused by mitochondrial calcium overload. *Ann N*  
1125 *Y Acad Sci* **1201**, 183–188.
- 1126 **Piccioli, Z. D. and Littleton, J. T.** (2014). Retrograde BMP Signaling Modulates Rapid Activity-  
1127 Dependent Synaptic Growth via Presynaptic LIM Kinase Regulation of Cofilin. *J Neurosci* **34**,  
1128 4371–4381.
- 1129 **Prinz, A. A.** (2006). Insights from models of rhythmic motor systems. *Curr Opin Neurobiol* **16**, 615–  
1130 620.
- 1131 **Prinz, A. A., Bucher, D. and Marder, E.** (2004). Similar network activity from disparate circuit  
1132 parameters. *Nat Neurosci* **7**, 1345–1352.
- 1133 **Pulver, S. R., Pashkovski, S. L., Hornstein, N. J., Garrity, P. A. and Griffith, L. C.** (2009). Temporal  
1134 dynamics of neuronal activation by Channelrhodopsin-2 and TRPA1 determine behavioral  
1135 output in *Drosophila* larvae. *J Neurophysiol* **101**, 3075–3088.

- 1136 **Rharass, T., Lemcke, H., Lantow, M., Kuznetsov, S. A., Weiss, D. G. and Panáková, D.** (2014).  
1137 Ca<sup>2+</sup>-mediated mitochondrial reactive oxygen species metabolism augments Wnt/ $\beta$ -catenin  
1138 pathway activation to facilitate cell differentiation. *J Biol Chem* **289**, 27937–27951.
- 1139 **Rosenzweig, M., Brennan, K. M., Tayler, T. D., Phelps, P. O., Patapoutian, A. and Garrity, P. A.**  
1140 (2005). The Drosophila ortholog of vertebrate TRPA1 regulates thermotaxis. *Genes Dev* **19**, 419–  
1141 424.
- 1142 **Roy, B., Singh, A. P., Shetty, C., Chaudhary, V., North, A., Landgraf, M., VijayRaghavan, K. and**  
1143 **Rodrigues, V.** (2007). Metamorphosis of an identified serotonergic neuron in the Drosophila  
1144 olfactory system. *Neural development* **2**, 20.
- 1145 **Saitoh, M., Nishitoh, H., Fujii, M., Takeda, K., Tobiume, K., Sawada, Y., Kawabata, M., Miyazono,**  
1146 **K. and Ichijo, H.** (1998). Mammalian thioredoxin is a direct inhibitor of apoptosis signal-  
1147 regulating kinase (ASK) 1. *EMBO J* **17**, 2596–2606.
- 1148 **Sanyal, S., Narayanan, R., Consoulas, C. and Ramaswami, M.** (2003). Evidence for cell  
1149 autonomous AP1 function in regulation of Drosophila motor-neuron plasticity. *BMC neuroscience*  
1150 **4**, 20.
- 1151 **Sanyal, S., Sandstrom, D. J., Hoeffler, C. A. and Ramaswami, M.** (2002). AP-1 functions upstream of  
1152 CREB to control synaptic plasticity in Drosophila. *Nature* **416**, 870–874.
- 1153 **Schmitt, S., Evers, J. F., Duch, C., Scholz, M. and Obermayer, K.** (2004). New methods for the  
1154 computer-assisted 3-D reconstruction of neurons from confocal image stacks. *Neuroimage* **23**,  
1155 1283–1298.
- 1156 **Schneider-Mizell, C. M., Gerhard, S., Longair, M., Kazimiers, T., Li, F., Zwart, M. F., Champion, A.,**  
1157 **Midgley, F. M., Fetter, R. D., Saalfeld, S., et al.** (2016). Quantitative neuroanatomy for  
1158 connectomics in Drosophila. *Elife* **5**.
- 1159 **Serrano, F., Kolluri, N. S., Wientjes, F. B., Card, J. P. and Klann, E.** (2003). NADPH oxidase  
1160 immunoreactivity in the mouse brain. *Brain Res* **988**, 193–198.
- 1161 **Shearin, H. K., Macdonald, I. S., Spector, L. P. and Stowers, R. S.** (2014). Hexameric GFP and  
1162 mCherry Reporters for the Drosophila GAL4, Q, and LexA Transcription Systems. *Genetics* **196**,  
1163 951–960.
- 1164 **Sigrist, S. J., Reiff, D. F., Thiel, P. R., Steinert, J. R. and Schuster, C. M.** (2003). Experience-  
1165 dependent strengthening of Drosophila neuromuscular junctions. *J Neurosci* **23**, 6546–6556.
- 1166 **Sink, H. and Whittington, P. M.** (1991). Location and connectivity of abdominal motoneurons in the  
1167 embryo and larva of Drosophila melanogaster. *J Neurobiol* **22**, 298–311.
- 1168 **Sorce, S., Stocker, R., Seredenina, T., Holmdahl, R., Aguzzi, A., Chio, A., Depaulis, A., Heitz, F.,**  
1169 **Olofsson, P., Olsson, T., et al.** (2017). NADPH oxidases as drug targets and biomarkers in  
1170 neurodegenerative diseases: What is the evidence? *Free Radic Biol Med* **112**, 387–396.
- 1171 **Soriano, F. X., Baxter, P., Murray, L. M., Sporn, M. B., Gillingwater, T. H. and Hardingham, G. E.**  
1172 (2009). Transcriptional regulation of the AP-1 and Nrf2 target gene sulfiredoxin. *Mol. Cells* **27**,  
1173 279–282.
- 1174 **Spina, M. B. and Cohen, G.** (1989). Dopamine turnover and glutathione oxidation: implications for  
1175 Parkinson disease. *Proc Natl Acad Sci USA* **86**, 1398–1400.

- 1176 **Steuilet, P., Cabungcal, J.-H., Coyle, J., Didriksen, M., Gill, K., Grace, A. A., Hensch, T. K.,**  
1177 **LaMantia, A.-S., Lindemann, L., Maynard, T. M., et al.** (2017). Oxidative stress-driven  
1178 parvalbumin interneuron impairment as a common mechanism in models of schizophrenia. *Mol.*  
1179 *Psychiatry* **22**, 936–943.
- 1180 **Stewart, B. A., Atwood, H. L., Renger, J. J., Wang, J. and Wu, C. F.** (1994). Improved stability of  
1181 *Drosophila* larval neuromuscular preparations in haemolymph-like physiological solutions. *J*  
1182 *Comp Physiol A* **175**, 179–191.
- 1183 **Stuart, J. A., Maddalena, L. A., Merilovich, M. and Robb, E. L.** (2014). A midlife crisis for the  
1184 mitochondrial free radical theory of aging. *Longev Healthspan* **3**, 4.
- 1185 **Sugie, A., Hakeda-Suzuki, S., Suzuki, E., Silies, M., Shimozone, M., Möhl, C., Suzuki, T. and**  
1186 **Tavosanis, G.** (2015). Molecular Remodeling of the Presynaptic Active Zone of *Drosophila*  
1187 Photoreceptors via Activity-Dependent Feedback. *Neuron* **86**, 711–725.
- 1188 **Sulkowski, M., Kim, Y.-J. and Serpe, M.** (2014). Postsynaptic glutamate receptors regulate local  
1189 BMP signaling at the *Drosophila* neuromuscular junction. *Development* **141**, 436–447.
- 1190 **Tejada-Simon, M. V., Serrano, F., Villasana, L. E., Kanterewicz, B. I., Wu, G. Y., Quinn, M. T. and**  
1191 **Klann, E.** (2005). Synaptic localization of a functional NADPH oxidase in the mouse  
1192 hippocampus. *Molecular and Cellular Neuroscience* **29**, 97–106.
- 1193 **Thiels, E., Urban, N. N., Gonzalez-Burgos, G. R., Kanterewicz, B. I., Barrionuevo, G., Chu, C. T.,**  
1194 **Oury, T. D. and Klann, E.** (2000). Impairment of long-term potentiation and associative  
1195 memory in mice that overexpress extracellular superoxide dismutase. *J Neurosci* **20**, 7631–7639.
- 1196 **Tirone, F. and Cox, J. A.** (2007). NADPH oxidase 5 (NOX5) interacts with and is regulated by  
1197 calmodulin. *FEBS Lett* **581**, 1202–1208.
- 1198 **Tonks, N. K.** (2005). Redox redux: revisiting PTPs and the control of cell signaling. *Cell* **121**, 667–670.
- 1199 **Tonks, N. K.** (2006). Protein tyrosine phosphatases: from genes, to function, to disease. *Nat Rev Mol*  
1200 *Cell Biol* **7**, 833–846.
- 1201 **Tripodi, M., Evers, J. F., Mauss, A., Bate, M. and Landgraf, M.** (2008). Structural homeostasis:  
1202 compensatory adjustments of dendritic arbor geometry in response to variations of synaptic  
1203 input. *PLoS Biol* **6**, e260.
- 1204 **Tsai, P.-I., Wang, M., Kao, H.-H., Cheng, Y.-J., Lin, Y.-J., Chen, R.-H. and Chien, C.-T.** (2012).  
1205 Activity-dependent retrograde laminin A signaling regulates synapse growth at *Drosophila*  
1206 neuromuscular junctions. *Proc Natl Acad Sci U S A* **109**, 17699–17704.
- 1207 **Ueda, A. and Wu, C.-F.** (2015). The role of cAMP in synaptic homeostasis in response to  
1208 environmental temperature challenges and hyperexcitability mutations. *Front Cell Neurosci* **9**,  
1209 10.
- 1210 **Waak, J., Weber, S. S., Görner, K., Schall, C., Ichijo, H., Stehle, T. and Kahle, P. J.** (2009). Oxidizable  
1211 residues mediating protein stability and cytoprotective interaction of DJ-1 with apoptosis signal-  
1212 regulating kinase 1. *J Biol Chem* **284**, 14245–14257.
- 1213 **Wagh, D. A., Rasse, T. M., Asan, E., Hofbauer, A., Schwenkert, I., Dürrbeck, H., Buchner, S.,**  
1214 **Dabauvalle, M.-C., Schmidt, M. and Qin, G.** (2006). Bruchpilot, a Protein with Homology to

1215 ELKS/CAST, Is Required for Structural Integrity and Function of Synaptic Active Zones in  
1216 *Drosophila*. *Neuron* **49**, 833–844.

1217 **Walker, J. A., Gouzi, J. Y., Long, J. B., Huang, S., Maher, R. C., Xia, H., Khalil, K., Ray, A., Van**  
1218 **Vector, D., Bernardis, R., et al.** (2013). Genetic and Functional Studies Implicate Synaptic  
1219 Overgrowth and Ring Gland cAMP/PKA Signaling Defects in the *Drosophila melanogaster*  
1220 Neurofibromatosis-1 Growth Deficiency. *PLoS Genet* **9**, e1003958.

1221 **Wang, T., Hauswirth, A. G., Tong, A., Dickman, D. K. and Davis, G. W.** (2014). Endostatin Is a  
1222 Trans-Synaptic Signal for Homeostatic Synaptic Plasticity. *Neuron*.

1223 **Weyhersmüller, A., Hallermann, S., Wagner, N. and Eilers, J.** (2011). Rapid active zone remodeling  
1224 during synaptic plasticity. *J Neurosci* **31**, 6041–6052.

1225 **Wilson, C., Muñoz-Palma, E., Henríquez, D. R., Palmisano, I., Núñez, M. T., Di Giovanni, S. and**  
1226 **González-Billault, C.** (2016). A Feed-Forward Mechanism Involving the NOX Complex and RyR-  
1227 Mediated Ca<sup>2+</sup> Release During Axonal Specification. *J Neurosci* **36**, 11107–11119.

1228 **Wilson, C., Núñez, M. T. and González-Billault, C.** (2015). Contribution of NADPH oxidase to the  
1229 establishment of hippocampal neuronal polarity in culture. *J Cell Sci* **128**, 2989–2995.

1230 **Wolfram, V. and Baines, R. A.** (2013). Blurring the boundaries: developmental and activity-  
1231 dependent determinants of neural circuits. *Trends Neurosci*.

1232 **Yeates, C. J., Zwiefelhofer, D. J. and Frank, C. A.** (2017). The Maintenance of Synaptic Homeostasis  
1233 at the *Drosophila* Neuromuscular Junction Is Reversible and Sensitive to High Temperature.  
1234 *eNeuro* **4**, ENEURO.0220–17.2017.

1235 **Younger, M. A., Müller, M., Tong, A., Pym, E. C. and Davis, G. W.** (2013). A presynaptic ENaC  
1236 channel drives homeostatic plasticity. *Neuron* **79**, 1183–1196.

1237 **Zhong, Y. and Wu, C.-F.** (2004). Neuronal Activity and Adenylyl Cyclase in Environment-Dependent  
1238 Plasticity of Axonal Outgrowth in *Drosophila*. *J Neurosci* **24**, 1439–1445.

1239 **Zhu, X.-H., Qiao, H., Du, F., Xiong, Q., Liu, X., Zhang, X., Ugurbil, K. and Chen, W.** (2012).  
1240 Quantitative imaging of energy expenditure in human brain. *Neuroimage* **60**, 2107–2117.

1241 **Zwart, M. F., Pulver, S. R., Truman, J. W., Fushiki, A., Fetter, R. D., Cardona, A. and Landgraf, M.**  
1242 (2016). Selective Inhibition Mediates the Sequential Recruitment of Motor Pools. *Neuron* **91**,  
1243 944.

1244 **Zwart, M. F., Randlett, O., Evers, J. F. and Landgraf, M.** (2013). Dendritic growth gated by a steroid  
1245 hormone receptor underlies increases in activity in the developing *Drosophila* locomotor  
1246 system. *Proc Natl Acad Sci U S A*.

1247

1248

1249